# Table of Contents

# CHAPTER 3:
# USING CONDUCTION VELOCITY TO ASSESS FATIGUE

## 3.1 MOTIVATION FOR EXAMINATION

One of the major influences on the power spectrum during fatigue is a decrease in velocity of the electrical signals propagating along the muscle fibres. This decrease in CV, caused by changes in electrochemical metabolite concentrations with the muscle's surrounding tissues, is manifested as an expansion of the MES in time which is reflected as a compression of the power spectrum. Thus, an alternative to tracking fatigue indirectly through power spectral parameters is to measure CV directly. While this is a more difficult measurement to make, it may be more resilient to the effects of dynamic factors.

The effects of muscle force and joint angle on power spectral parameters are mostly a result of changes during dynamic contractions, in the geometrical arrangement of the active motor units with respect to each other and to the detecting electrodes [28]. First, since the surface MES reflects a summation of activity in the detectable region, as the relative positioning between muscle fibres changes, the surface MES shape may change inducing modifications in the MES power spectrum [8, 12]. Also, tissue between the active fibres and measuring electrodes acts as a low-pass filter, modifying the spectrum further [8, 12].

As these features are altered during dynamic contractions they produce striking effects on the power spectrum and related parameters such as MF. While it is difficult to examine the effects under dynamic conditions because of the high variability associated with instantaneous power spectral estimates, the effects can be inferred by comparing estimates obtained during different levels of static contractions. Figure 3-1 is such an example taken from the brachial biceps at five joint angles and three force levels [28].

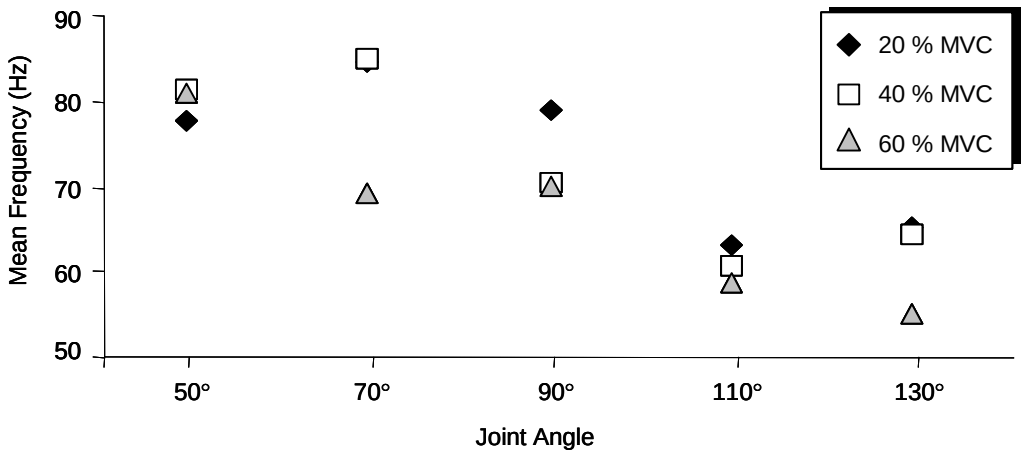


**Figure 3-1: MF values vs joint angle from MES obtained from the brachial biceps during static contractions at three force levels (based upon % Maximum Voluntary Contractions (MVC)). Standard deviations (±1) are shown where resolvable (> 2 Hz).**

Commonly, estimating CV with surface MES is achieved by taking the cross-correlation of two measurements separated along the MES propagation path by a known distance. The time shift in this cross-correlation from zero represents the time taken by the propagating signal to travel the separation distance '$\tau_d$';

thus dividing this distance '$d$' by the time yields CV. This methodology is summarized in Figure 3-2.

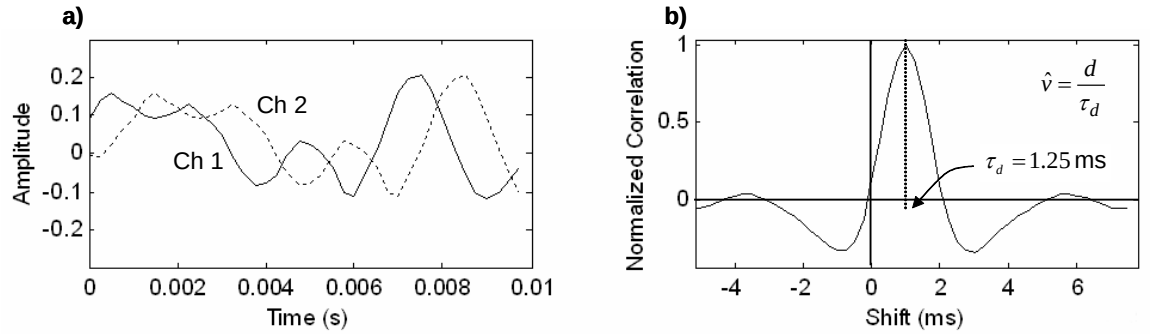


**Figure 3-2: Summary of the cross-correlation method for measuring CV. a) Surface MES measured from two channels at different locations along the propagating path. b) Cross-correlation between the signals in a).**

Since CV is determined by comparing two channels of MES ideally under the same conditions, the factors that affect power spectral estimates may not influence CV estimation. Nevertheless, because the MES is a summation of activity across multiple fibres, as with power spectral estimates, CV estimates obtained using the cross-correlation technique reflect an average CV across the active fibres. This average CV may be altered as new fibres are introduced with recruitment to increase force level, or as new fibres enter the detectable regions of the measuring electrodes because of changes in joint angle.

Other considerations may be even more problematic. The accuracy of a CV estimate depends upon at least three assumptions. The first is that both channels are placed along the length of the active muscle fibres. Since all fibres in a muscle are not completely parallel, this assumption can never be perfectly

realized. However, choosing a small channel spacing can limit this misalignment to an acceptable level [21].

The second assumption is that both channels are placed on the same side of the IZ. Under static conditions, channel placement can be chosen to realize this assumption. However, whether or not it is met under dynamic conditions depends on the effect that joint angle has on the relative position of the channels with respect to the IZ. Muscle force may confound this effect by introducing new active fibres which may further alter the relative positions.

The third assumption is that the fibres are sufficiently long to render the effects of action potential origination and extinction (collectively known as non-propagating end-effects) insignificant. For most muscles, there are joint angles at which this assumption can be realized. However, under dynamic conditions, as muscle length shortens to change joint angle, this assumption may not always be valid.

Muscle force and/or joint angle may not affect CV estimates in the same way that they affect power spectral parameters. However, they may affect CV in different ways making it equally susceptible to variability while estimating under dynamic contractions. Experimental work was warranted to determine this susceptibility.

## 3.2 EFFECTS OF DYNAMIC PARAMETERS ON CONDUCTION VELOCITY ESTIMATION – EXPERIMENT 1

### 3.2-1 Purpose

To examine the effects of muscle force and joint angle on CV estimation, a test was conducted to compare CV values obtained using the cross-correlation technique on two channels of static MES data generated from the brachial biceps. Data were collected with the elbow held at five joint angles. The muscle resisted three loads at each angle. The loads were determined as a percentage of a joint angle specific maximal voluntary contraction (MVC). While the values used for comparison in this experiment were not obtained under dynamic conditions, the effects of the dynamic factors could be inferred from the static results.

### 3.2-2 Method

The apparatus used in this experiment consisted of a large disc attached to a central pulley at its axis as depicted in Figure 3-3. The central pulley and disc were supported with a frame which allowed participants to rest their upper arms upon a platform with elbow aligned with the pulley-disc axis. Participants could then apply a force to a handle attached to the disc with the forearm supinated, at any specified elbow joint angle. By attaching a mass to the pulley, a specified force could be applied perpendicular to the forearm regardless of the joint angle held by the participant. Furthermore, by fastening the pulley in a particular

position, the forearm could apply any force perpendicular to the opposing tension while held at a particular joint angle.

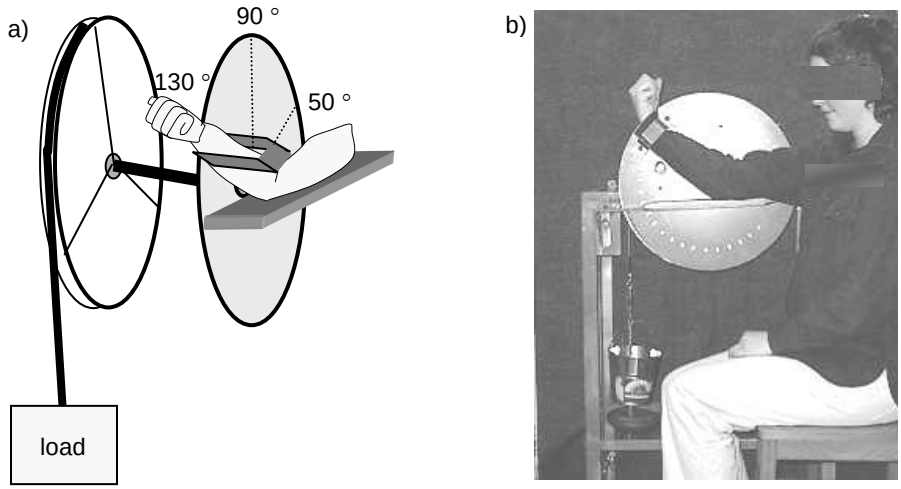


**Figure 3-3: Central pulley apparatus used in experiment 1 to apply loads at specified joint angles.**

Using the central pulley apparatus in the fastened mode, MVC measurements were obtained for each participant at 50°, 70°, 90°, 110° and 130° (relative to 180° at full elbow extension). To obtain the MVC value, participants were encouraged to pull as hard as possible against the fastened pulley. The pulley was fastened via a cable to a LC105 Aluminum 'S' Beam Load Cell which output a voltage proportional to the force being exerted. This process was repeated three times for proper training, with one minute intervals between each trial. The highest value of the trials was used as the MVC.

One day after the MVC test, participants returned for signal acquisition. Using the central pulley apparatus, participants were instructed to hold the disc at 50°,

70°, 90°, 110° and 130° against loads equivalent to 20%, 50% and 70% of their MVCs. Each angle-force combination was held for 15 seconds and a one minute rest interval between each combination was imposed. The order in which the participants engaged in each combination was randomized.

The MES was recorded from the brachial biceps using a flexible bar electrode array with three 0.5 mm x 10 mm bars permanently fixed 5.0 mm apart. The bars were configured in single differential mode yielding two channels with an effective separation of 5.0 mm. Before electrodes were placed, the skin surface on which the array mounted was cleansed with rubbing alcohol and treated with conducting gel. The array was placed on the short head of the muscle, midway between the belly and the tendon on the proximal side and secured with a breathable elastic cuff. The reference electrode was placed on the forearm.

Both MES channels were processed identically first through a pre-amplifier configuration described previously by Lovely [95] and then through a Tektronix AM502 differential amplifier. The combined gain was set at 2000 and the low and high cut-off frequencies of each amplifier were set to 1 Hz and 1000 Hz respectively. This rather liberal bandwidth was chosen to accommodate the broad gain transition band of the amplifiers. From the amplifiers, each signal was sent to an oscilloscope for display and through an anti-aliasing filter with the cut-off frequency set to 500 Hz. Finally, the signals were sampled at a rate of 5000 Hz/channel with a resolution of 2.4 mV/bit using a CIO-DAS16/330I 12 bit A/D board.

In total, 15 data records from each channel were obtained for each participant; one for each angle-force combination. Each 15 s data record was interpolated using a linear low-pass interpolator filter to increase the time resolution from 1/5000 to 1/15000. Then each interpolated record was split into three 5 s segments. Finally, the cross-correlation between channels was obtained for each segment, the delay was determined from the shift in the cross-correlation peak from zero, and a CV value was calculated based on the delay and channel spacing. This process yielded three CV values for each angle-force combination, based on the 5 s segments. Data were collected from three female participants aged 22, 25 and 29 and two male participants aged 22 and 60.

### 3.2-3 Results

Table 3-1 lists the MVC results obtained for each of the five participants (P1-P5) in this experiment:

| Angle | P1 | P2 | P3 | P4 | P5 |
|---|---|---|---|---|---|
| **50°** | 11.24 kg | 13.47 kg | 7.98 kg | 23.50 kg | 21.28 kg |
| **70°** | 11.61 kg | 13.84 kg | 7.43 kg | 25.74 kg | 21.65 kg |
| **90°** | 11.61 kg | 13.10 kg | 7.98 kg | 25.74 kg | 20.53 kg |
| **110°** | 10.12 kg | 12.73kg | 7.70 kg | 25.00kg | 20.53 kg |
| **130°** | 9.38 kg | 11.61kg | 6.88 kg | 21.28 kg | 16.81kg |

**Table 3-1: MVC Results from Experiment 1**

Figure 3-4 depicts the CV vs Joint Angle results for each participant. In each plot, the means of the three CV values calculated for each angle-force combination are plotted. Error bars representing $\pm$ 1 standard deviation are also

shown where resolvable (> 0.5 m/s). Outliers have been depicted out of scale with their mean values and standard deviations indicated in brackets.

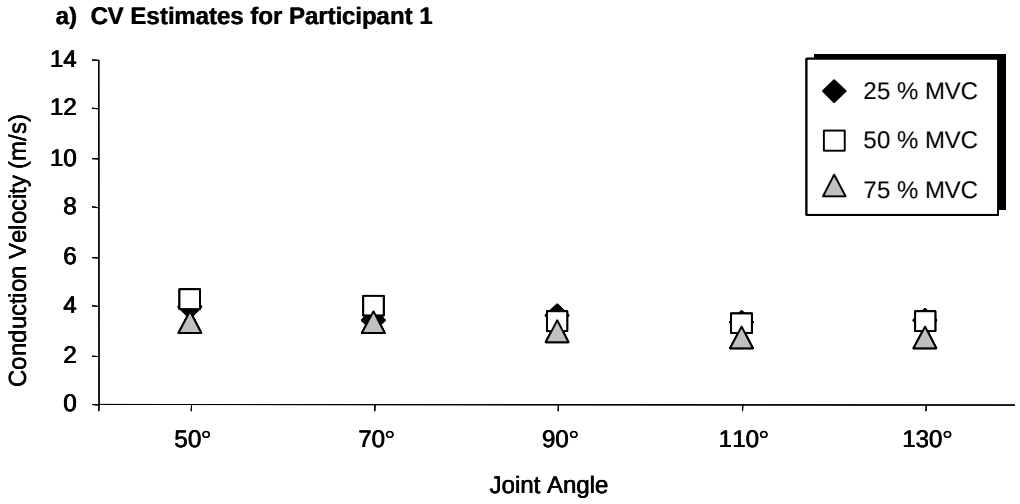


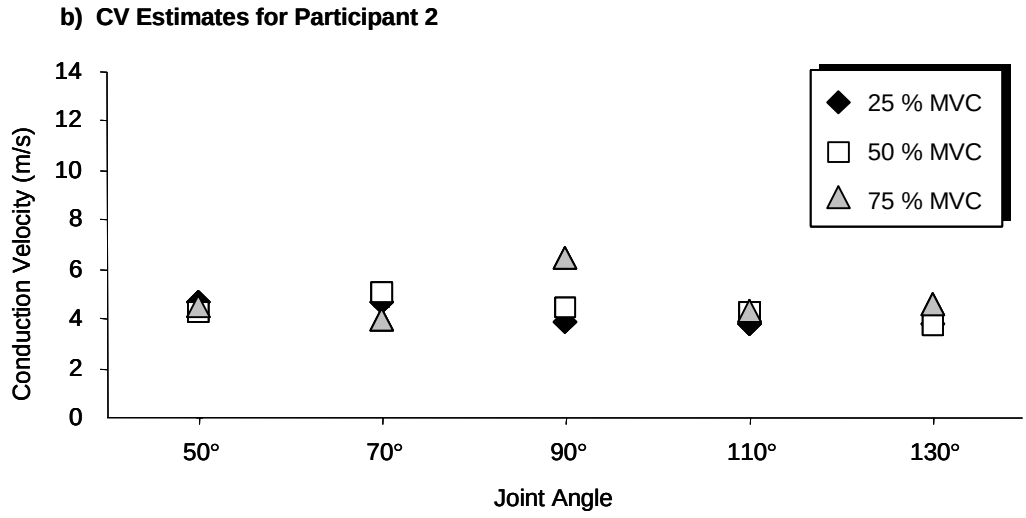


**Figure 3-4: Continued on next page...**

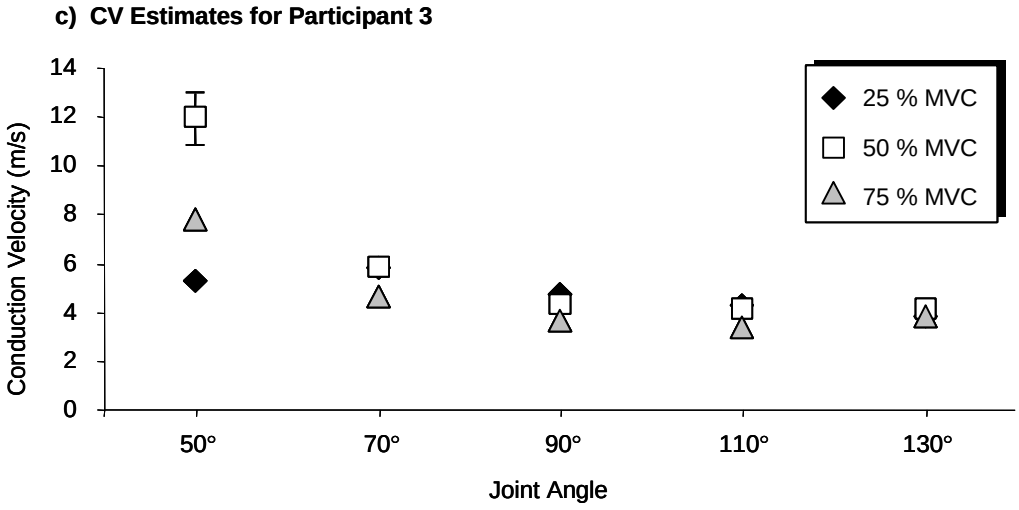


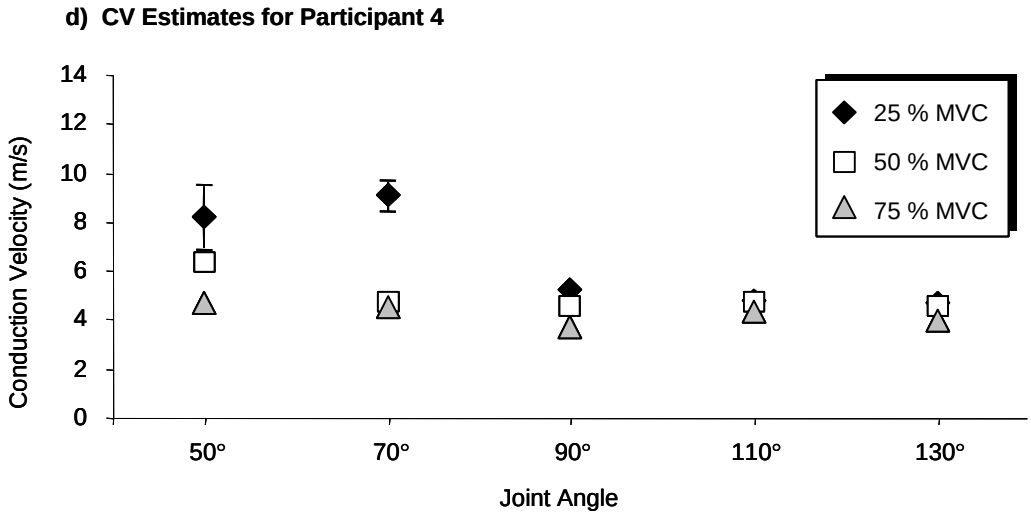


**Figure 3-4: Continued on next page...**

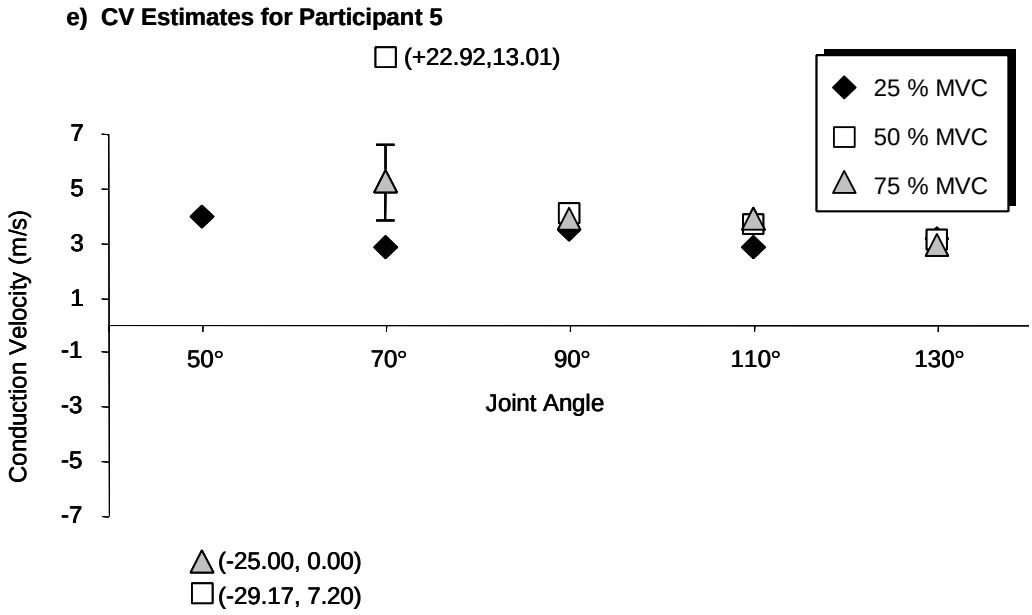


**Figure 3-4 CV estimates from experiment 1. Each data point represents the mean of three trials at the specified angle-force combination. Standard deviation bars (±1) are indicated where resolvable (>0.5m/s). Outliers are depicted at the boundaries with their mean values and standard deviations listed in brackets.**

A statistical analysis of the data pooled across participants revealed statistically significant effects from both joint angle (ANOVA; $\alpha = 0.05$, $p < 0.001$) and muscle force (ANOVA; $\alpha = 0.05$, $p < 0.001$). However a post-hoc Bonferroni analysis revealed that the effects were only evident in the data from angles 50° and 70°. The results of these analyses held, even when participant 5 was removed from the data set to account for the outliers associated with this participant (see Figure 3-4e).

### 3.2-4 Explanation of Results

While the variability in CV estimates for the first two participants in this experiment was low ($\sigma^2$<0.20 m/s, with respect to mean across joint angle and muscle force) this was not the case for all participants. As indicated in Figure 3-4c-e, for participants 3 and 4, the variability in CV estimates increased ($\sigma^2$>2 m/s), and for participant 5, outliers were clearly evident ($\sigma^2$>100 m/s).

Intriguingly, the effects of joint angle and muscle force on the CV estimates in this experiment were only evident in the data collected at 50° and 70°. Because these joint angles correspond to near maximal shortening of the muscle, at these angles the electrodes are brought in closest proximity to muscle fibre innervations and terminations. It was therefore speculated that the MES manifestations of action potential origination and extinction were primary contributors to the effects noted, along with cross-correlation degradation caused by electrodes traversing the IZ.

Using the cross-correlation technique, electrode location with respect to the IZ and fibre termination regions is a critical factor in meeting the assumptions required to obtain accurate CV estimates. Since muscle fibres are finite in length, end-effects, which manifest as non-propagating components in MES, can introduce a non-delay element into the cross-correlation which biases the CV estimate. These effects have been shown to increase as the depth of active muscle fibres increases and as electrodes get closer to the IZ or regions of fibre

termination [96, 97]. Also, as expected, striking effects have been shown on the cross-correlation which increase the variability of CV estimates as electrodes align with or traverse the IZ.

As joint angle decreases, muscle fibre length decreases. Also, the IZ has been shown to migrate towards the measuring electrodes [98, 99]. These changes are reflected in MES measurements as changes in electrode location. If substantial, they can cause increased bias and/or variability in CV estimations rendering CV difficult to measure during dynamic contractions. Because different motor units are recruited at different force levels, IZ and muscle fibre termination regions may also vary in location with muscle force. When this happens, muscle force becomes a confounding factor contributing to the inaccuracy and/or imprecision of CV estimation during dynamic contractions.

Two tactics may be employed to reduce the variability in CV estimates as joint angle and/or muscle force changes. First, electrodes can be configured as double differential pairs to reduce the non-propagating components in the MES [86, 100] since these components are common to both channels. Second, when possible, electrodes may be strategically placed so that the conditions necessary to measure CV are met regardless of joint angle. Unfortunately, there is no guarantee that such an electrode position will always be available.

### 3.2-5 Conclusions

The effects of muscle force and joint angle on CV estimation were examined in this experiment. Results indicated that joint angles which corresponded to sufficiently decreased fibre lengths yielded biased estimates of CV which became increasingly more variable. Based on these observations, CV will not make a viable index of fatigue under dynamic conditions, unless the effects of muscle force and joint angle can be controlled. To determine the feasibility of controlling the effects, an examination of the influence of end-effects and IZ migration was warranted.

## 3.3 SIMULATING EFFECTS OF DYNAMIC FACTORS ON CONDUCTION VELOCITY

Based on the results of Experiment 1, end-effects and/or degradation of the cross-correlation due to electrodes traversing the IZ, hereon in termed 'electrode misplacement effects', are likely contributors to the influence that joint angle and muscle force have on CV estimates. Changes in CV caused by the recruitment of additional motor units made up of fibres with larger diameters may also be a contributing factor. However, this manifestation is unlikely in the brachial biceps as evidence suggests that CV varies within a narrow range in this muscle, despite the variation in fibre diameter [10]. To examine more closely the impact that end-effects and electrode misplacement effects have on CV estimation, a simulation based on MES modeling was conducted.

Using a model of a single fibre action potential (SFAP) previously developed by Gonzalez-Cueto and Parker [101], MES was simulated by summing SFAPs, taking into consideration individual fibre lengths, depths and IZ locations with respect to the recording electrodes. Then both end-effects and electrode misplacement effects could be independently scrutinized by varying parameters such as fibre length and depth, electrode location, electrode configuration, the number of fibres in a single motor unit and the number of motor units in a given MES.

## 3.3-1 Signal Modeling

### 3.3-1a The Single Fiber Action Potential

Figure 3-5 depicts the geometrical assumptions made to model a typical SFAP measured at the skin surface.

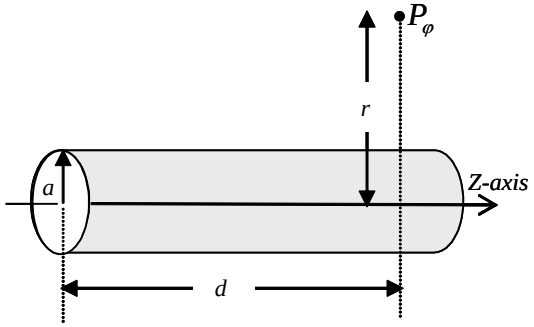


**Figure 3-5: Geometry used for modeling the extracellular potential at point '$P_\varphi$' due to a differential source located at z along a fibre. The fibre is assumed to (1) have a radius of 'a' and (2) have the z-axis as its longitudinal axis.**

In this depiction, a cylindrical fibre is assumed, and the *z-axis* represents the fibre's longitudinal axis while $a$ represents its radius. Since $P_\varphi$ represents the

point at which the extracellular potential is evaluated, $d$ represents the distance along the fibre axis between the source and the recording electrodes and $r$ represents the depth of the fibre.

To generate a SFAP, a double layer differential source as suggested by Plonsey [102] was convolved with a filtering function which took into consideration the field distribution properties of the source, bi-directional propagation of the source, depth of fibre, the location of the innervation point (IP) and the location of the left and right fibre terminations with respect to electrode location. This process simulated the extracellular potential generated by the propagating source as seen by recording electrodes at the skin surface. When transposed from spatial to temporal coordinates, the extracellular potential is described as a function in time as indicated in Equation 3-1, taken from Gonzalez-Cueto and Parker [101], who were guided originally by the work of Dimitrov and Dimitrova [107]:

$$\varphi(t) = K \cdot \left[ \int_0^{t_L} s(t-t') \cdot h\left(t' + \frac{d}{v}\right) \cdot dt' + \int_0^{t_R} s(t-t') \cdot h\left(t' - \frac{d}{v}\right) \cdot dt' \right] \qquad (3\text{-}1)$$

In Equation 3-1, $K$ represents a scaling factor dependent upon the ratio between intracellular and extracellular conductivities ($\sigma_i / \sigma_e$) and the square of the ratio between fibre diameter and CV ($\phi = a/v$):

$$K = \frac{1}{2} \frac{\sigma_i \phi^2}{4\sigma_e}, \qquad (3\text{-}1a)$$

$s(t)$ represents the differential source:

$$s(t) = \frac{\partial V_m(t)}{\partial t}, \tag{3-1b}$$

where $V_m(t)$ is the transmembrane potential and $h(t)$ represents the filter function which accounts for the transformation undergone by the field as it travels through tissue towards the recording electrodes. It is dependent upon fibre depth ($r$) and CV ($v$):

$$h(t) = \frac{t}{\left[\left[r/v\right]^2 + t^2\right]^{3/2}} \tag{3-1c}$$

In this model, the locations of IP and the fibre terminations are considered within the limits of integration, $t_R$ and $t_L$, which represent the time it takes the source to propagate from the IP to the right and left terminations, respectively. Also, when $d$ and $r$ vary, the extracellular potential becomes a function of these parameters as well as time, as indicated in Equation 3-2:

$$\varphi(t,r,d) = K \cdot \left[\int_{-\infty}^{+\infty} s(t-t') \cdot \left[h_L(t,d,r,t_L) + h_R(t,d,r,t_R) \cdot dt'\right]\right] \tag{3-2}$$

where

$$h_L(t,d,r,t_L) = \begin{cases} 0, & t < 0 \\ h\left(t + d/v\right) & 0 \le t \le t_L \\ 0, & t > t_L \end{cases} \tag{3-2a}$$

$$h_R(t,d,r,t_R) = \begin{cases} 0, & t < 0 \\ h\left(t - d/v\right) & 0 \le t \le t_R \\ 0, & t > t_R \end{cases} \qquad \text{(3-2b)}$$

To complete the generation of the SFAP, the source waveform was specified according to Gonzalez-Cueto and Parker [101] as defined and depicted in Figure 3-6.

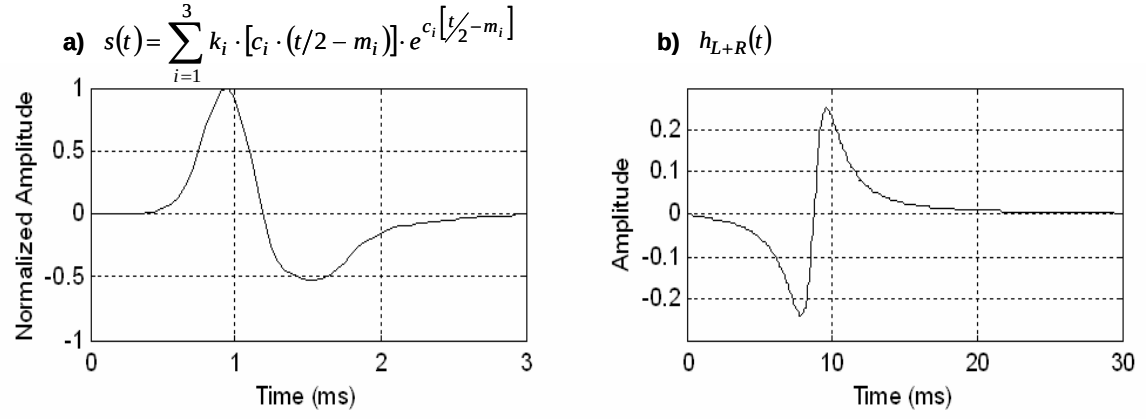


**Figure 3-6: a) Source used to model SFAP ($k_1$ = 51, $k_2$ = 72, $k_3$ = 18, $c_1$ = -64.00, $c_2$ = -28.41, $c_3$ = -11.09, $m_1$ = 0.54, $m_2$ = 0.66, $m_3$ = 0.86). b) Tissue filter used to model SFAP ($h_{L+R}(t) = h_L(t+d/v)+h_R(t-d/v)$ for d = 35mm, $t_L$ = 22.5 ms, $t_R$ = 30 ms, v = 4 m/s).**

### 3.3-1b The Motor Unit Action Potential

It is useful to examine end-effects and electrode misplacement effects at the SFAP level. From this perspective the effects are clear and quantifiable because a particular fibre length, depth and IP location may be specified. However, such an analysis is limited because it cannot take into account dispersion in the parameters across many fibres. Thus the analysis must be extended to the level of multiple fibres. To model a MUAP, single fibres were grouped and summed to

form motor units. Each fibre in a summation had its own values specified for the defining parameters. Figure 3-7 depicts the parameters and Table 3-2 describes them.

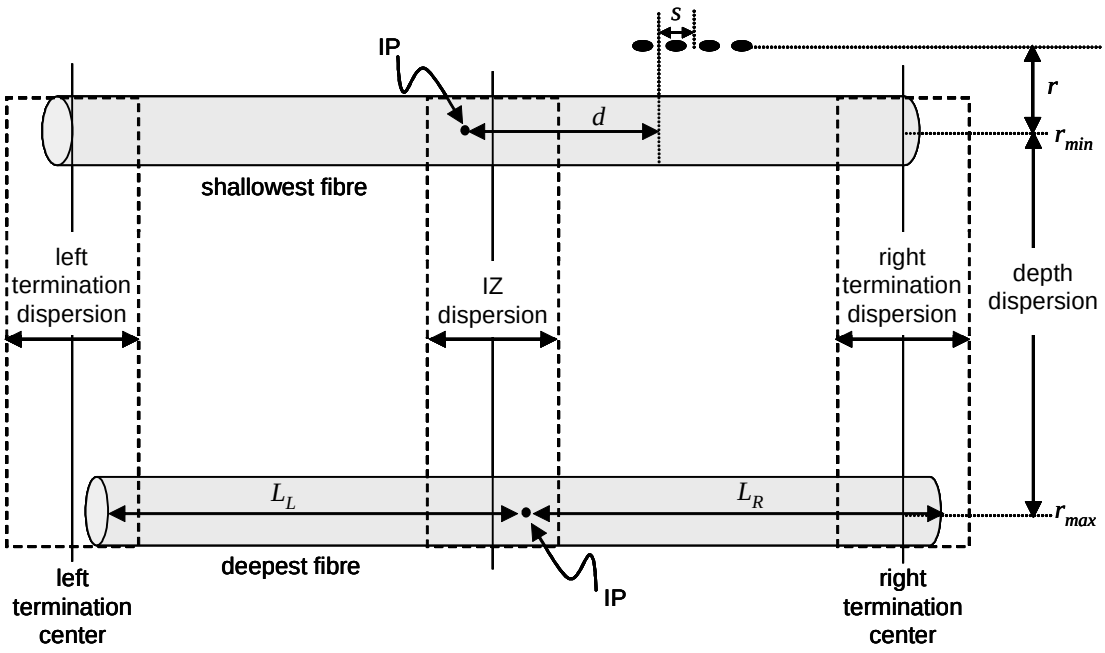


**Figure 3-7: MUAP Model Parameters**

| Parameter | Description |
|---|---|
| $s$ | Electrode spacing |
| $r$ | Depth of a given fibre:<br>• chosen relative to an average depth '$r_{ave}$' from a uniform distribution within the depth dispersion limits<br>• average depth chosen from uniform distribution between $r_{min}$ and $r_{max}$ |
| $d$ | Distance between IP of a given fibre and the closest electrode:<br>• IP location chosen relative to IZ center from a uniform distribution within the IZ dispersion limits |
| $L_R$ | Distance between IP of a given fibre and its right termination:<br>• fibre termination location chosen relative to right termination center from a uniform distribution within the right termination dispersion limits |
| $L_L$ | Distance between IP of a given fibre and its left termination :<br>• fibre termination location chosen relative to left termination center from a uniform distribution within the left termination dispersion limits |

**Table 3-2: List of SFAP Parameters used in MUAP Simulation**

Also shown in the figure and listed in the table is electrode spacing '$s$', which was independent of fibre and so common to all fibres. For a monopolar electrode configuration, this parameter measured the distance between adjacent channels. A bipolar electrode configuration was modeled by subtracting the right monopolar channel from the left; thus electrode spacing '$s$' measured the inter-electrode distance in the bipolar configuration which was also the effective distance between bipolar channels.

Since the same fibres are always stimulated in a given motor unit, an MUAPt can be formed by convolving the MUAP with a time-series of impulses representing the innervation process of that motor unit as indicated in Equation 3-3. This step was conducted so that the characteristics of the innervation process could be considered in the analysis.

$$\varphi_{MUAPt}(t) = \varphi_{MUAP}(t) * \sum_{k=1}^{T} \delta(t - t_k) \tag{3-3}$$

In this equation,

$$t_k = \sum_{l=1}^{k} x_l \quad for \;\; k = 1,2,3...T \tag{3-3a}$$

where $x_l$ is a random variable representing the $l^{th}$ interpulse interval (IPI). The probability distribution governing the IPI has been shown to be inconsistent. Based on empirical evidence it has previously been modeled with Poisson [14],

Wiebel [15] and Gaussian distributions [17, 18]. Regardless of the distribution observed, only a weak, if any, correlation has been observed between adjacent IPIs [103, 104, 105]. An independent Gaussian distribution was utilized in this model.

### 3.3-1c The Myoelectric Signal

To model a typical MES segment, many independently generated MUAPts were summed. The entire modeling process is summarized in Figure 3-8.

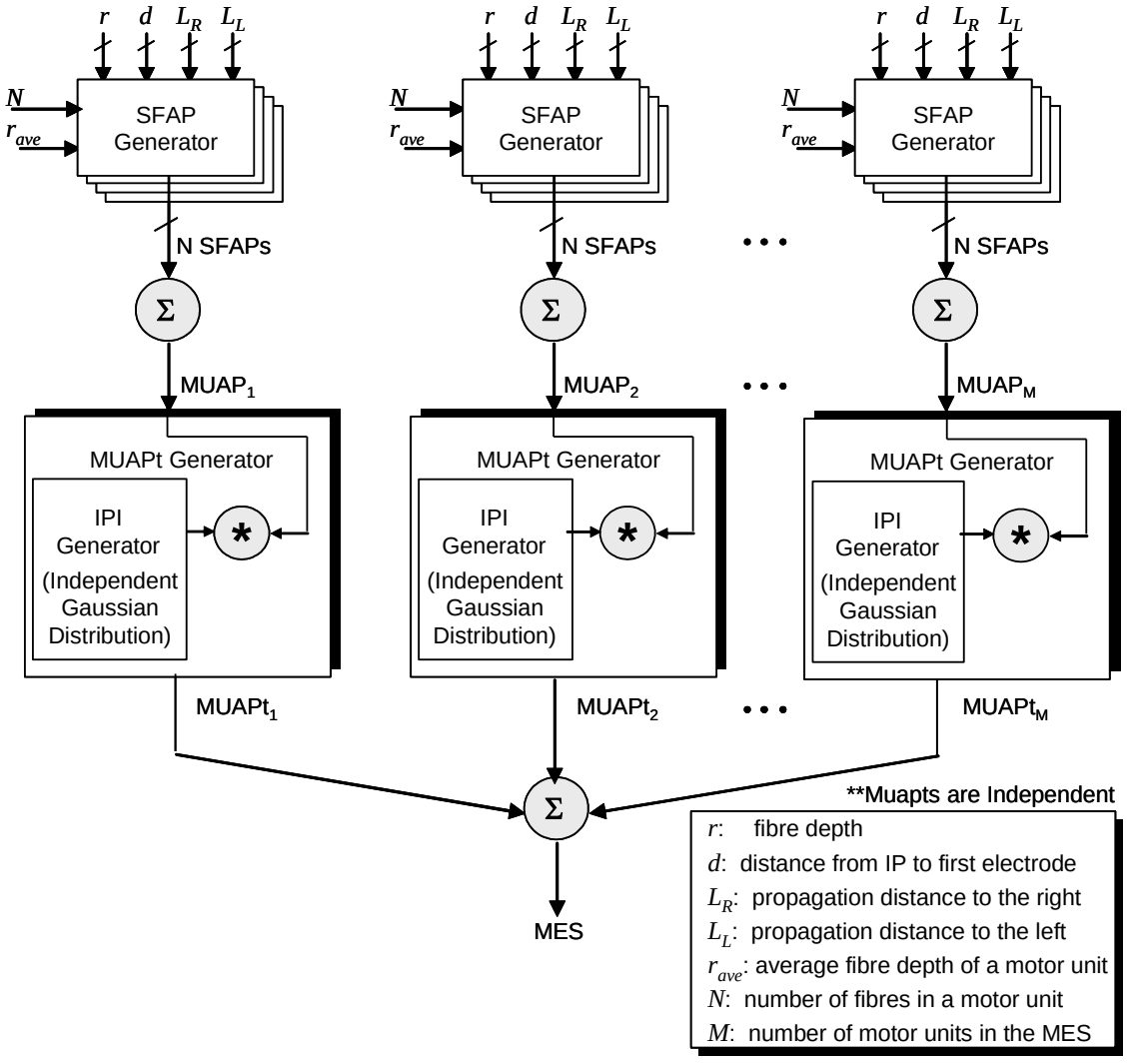


**Figure 3-8: Summary of MES Modeling Process**

## 3.3-2 Demonstrating End-effects

### 3.3-2a The Single Fibre Action Potential

Figure 3-10 depicts a simulated SFAP as measured by two channels at three locations along the fibre axis ($d = 5, 35 \; and \; 75 \; mm$ with respect to the IP, as depicted in Figure 3-9). Both monopolar and bipolar simulations are depicted. In this example $s = 5\,mm$, $r = 15\,mm$, $L_L = 120\ mm$, $L_R = 90\ mm$, and $v = 4\,m/s$.

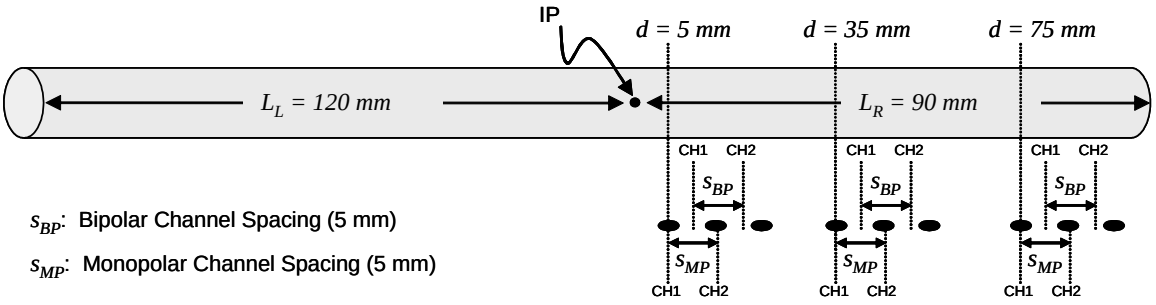


**Figure 3-9: Fibre Parameters for Example Depicted in Figure 3-10**

Figure 3-10b) represents the SFAP measured at an optimal electrode location for the parameters specified in this example. The location of the first electrode in the array is 35 mm away from the IP and each subsequent electrode is another 5 mm away. At this distance, the end-effect due to signal origination is negligible at both channels and the propagating component of the SFAP waveform at one channel is a shifted version of the propagating waveform at the other channel. This is true for both the monopolar and bipolar electrode configurations.

The location of the first electrode in the array is 55 mm and 155 mm from the right and left fibre terminations, respectively. While the larger distance is long

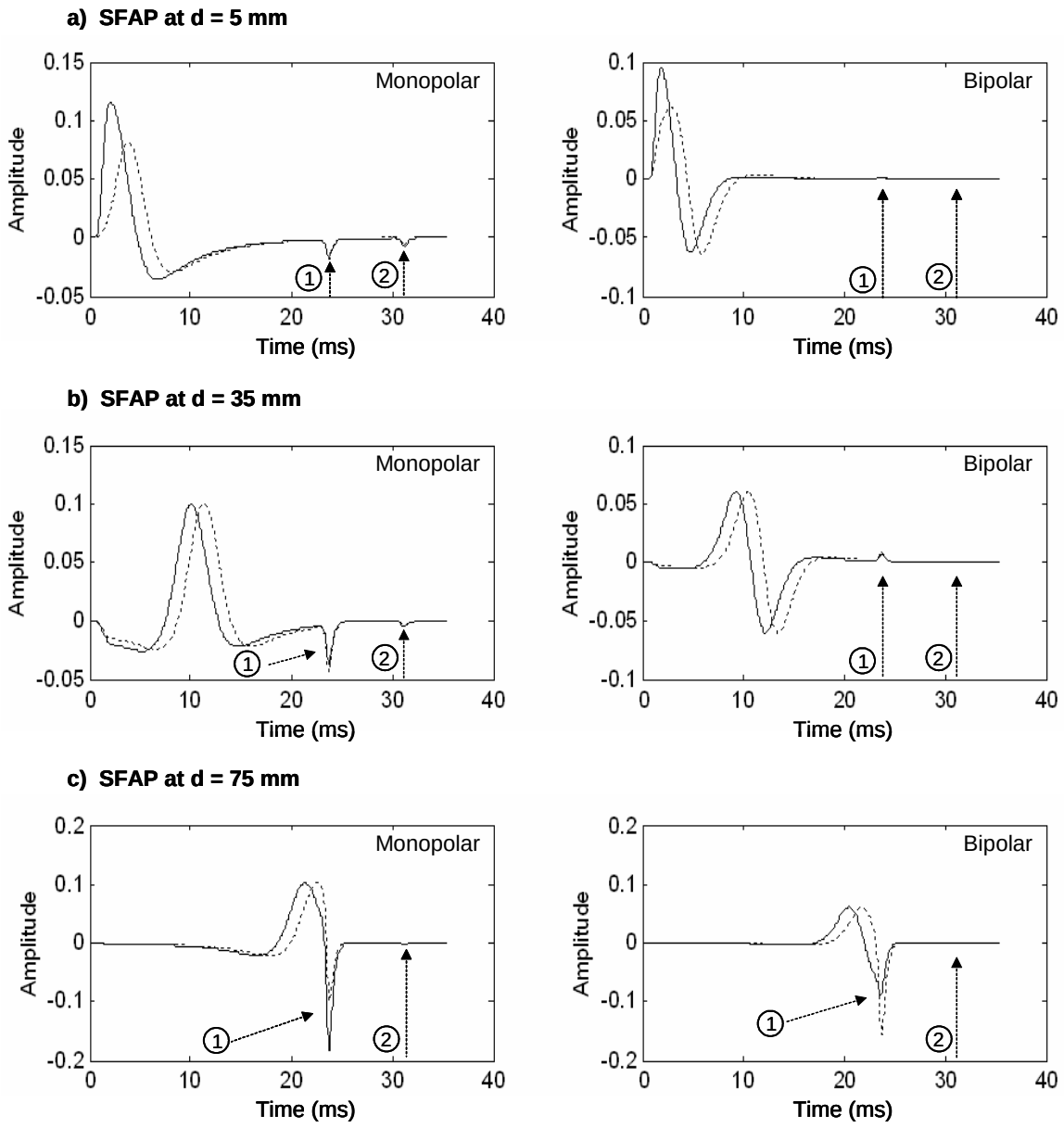


**Figure 3-10: Simulated SFAP at three electrode locations demonstrating end-effects a) d = 5 mm b) d = 35 mm c) d = 75 mm. Monopolar and bipolar simulations are shown with two channels superimposed ( CH1 —, CH2 --- , s = 5 mm, r = 15 mm, $L_R$ = 90 mm, $L_L$ = 120 mm, v = 4 m/s, arrows indicate ① proximal and ② distal end-effects).**

enough to render the end-effect from the farthest termination (②) almost negligible, there is an apparent non-propagating component (①) clearly visible, beginning at the time it would take the source to travel the nearest termination

($t_R = 90/4 = 22.5\,ms$) in both the monopolar and bipolar measurements. Note that this signal component is located at $t_R$, regardless of the channel from which the signal was acquired. Thus, even at this optimal electrode location, end-effects due to fibre termination are apparent in the SFAP.

Figure 3-10a) and Figure 3-10c) represent the SFAP measured at extreme electrode locations. When the first electrode in the array is located only 5 mm from the IP (Figure 3-10a), end-effects due to signal origination are superimposed on the propagating component of the SFAP changing its shape from one channel to the next. This was observed in both monopolar and bipolar measurements. Signal termination effects were also observed in the monopolar signal, not only from the right termination (①), but also from the left (②, $t_L = 120/4 = 30\ ms$).

On the other extreme, when the last electrode in the array is located only 5 mm from the right fibre termination (Figure 3-10c), end-effects due to signal termination are superimposed on the propagating component of the SFAP changing its shape from one channel to the next. In this case, at least a portion of the end-effect (①) is sufficiently large to distinguish it from the propagating component despite the superposition, especially in the monopolar measurement.

While it is clear that at least some non-propagating end-effects are likely to occur during a typical SFAP measurement, it is not apparent how these effects impact on CV estimation. To determine this, cross-correlations between the channels

were obtained, and the peaks of the delay elements were located. The cross-correlations and peak locations ( $\tau_d = s/\hat{v}$ ) are depicted in Figure 3-11.

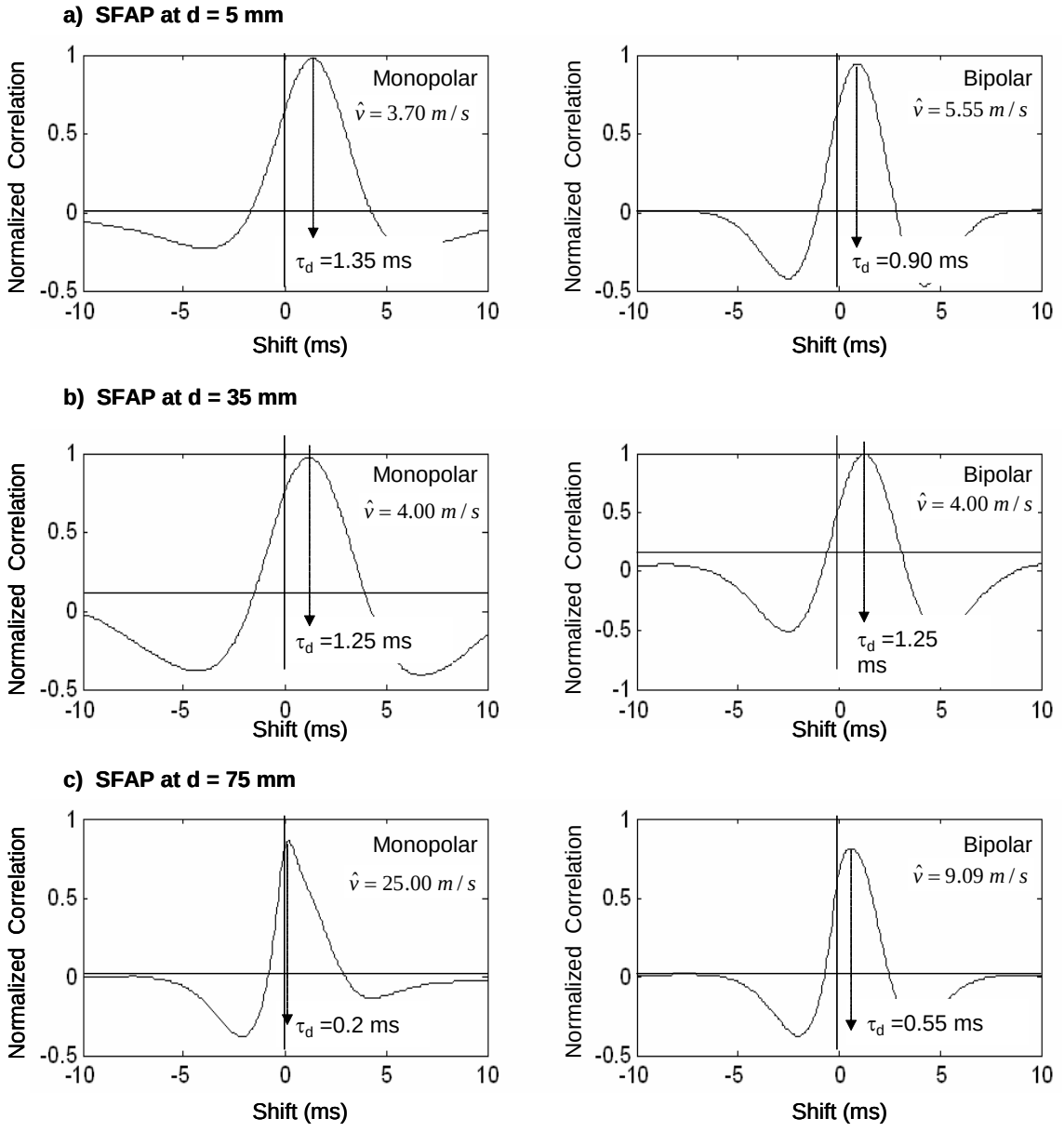


**Figure 3-11: Cross-correlation between simulated SFAP from two channels at three electrode locations a) d = 5 mm b) d = 35 mm c) d = 75 mm. Monopolar and bipolar simulations are shown (s = 5 mm, r = 15 mm, $L_R$ = 90 mm, $L_L$ = 120 mm, v = 4 m/s) and shift from zero ($\tau_d$) and resulting estimated CV ( $\hat{v}$ ) are indicated.**

It is apparent from Figure 3-11 that CV is estimated without bias when electrodes are placed optimally in this example (middle plots). However, the end-effects due to signal origination (top plots) and to a larger extent the end-effects due to signal termination (bottom plots) show bias in the estimation. Furthermore, while the bipolar configuration does attenuate the effects, the biases introduced under the extremes examined in this example are problematic, even in the bipolar measurement.

Figure 3-12 expands the analysis by considering more electrode locations and more fibre depths:

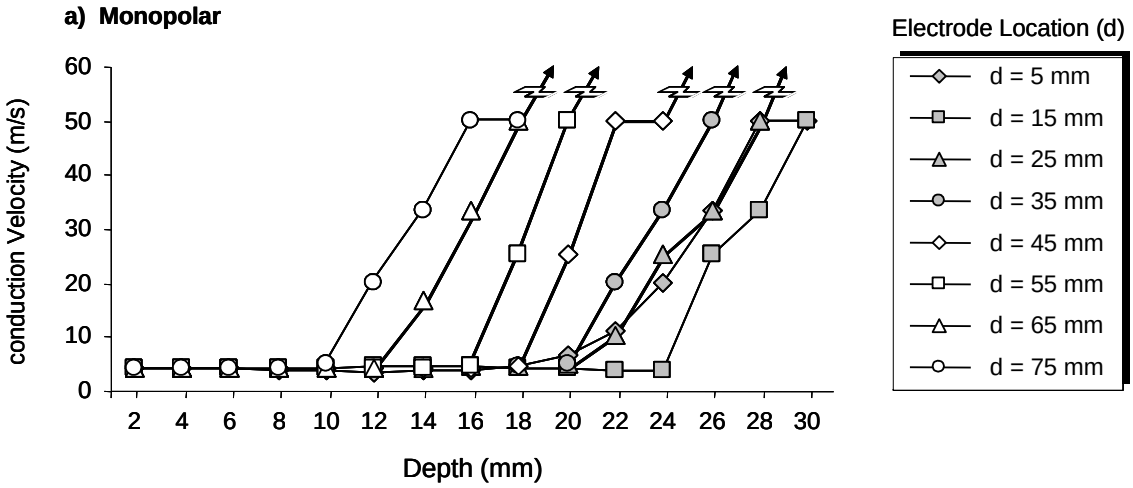


**Figure 3-12: Continued on next page...**

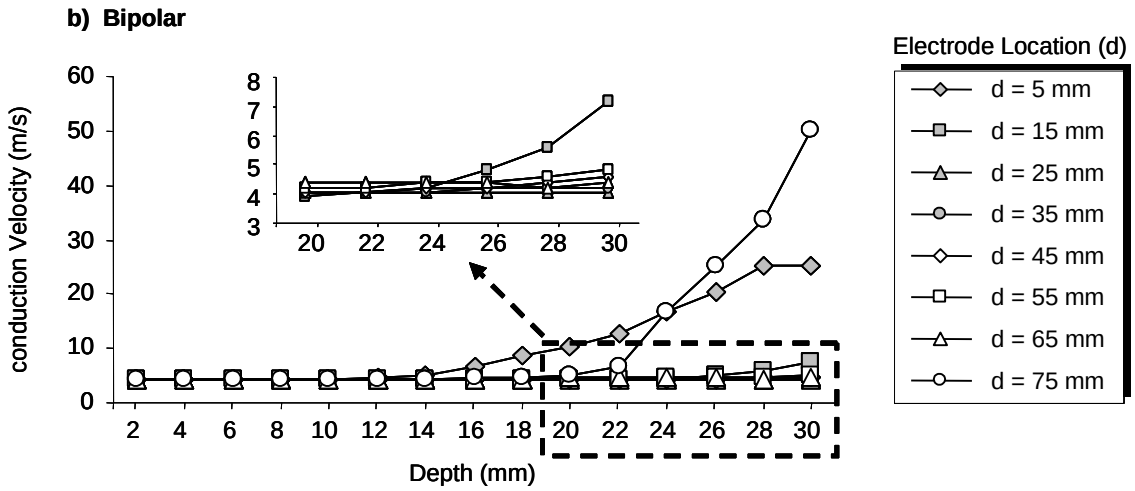


**Figure 3-12: CV estimates from simulated SFAP at various fibre depths and electrode locations (s = 5mm, $L_R$ = 90 mm, $L_L$ = 120 mm, v = 4 m/s). a) Monopolar simulation (the arrows indicate that estimates increased to >100 m/s at next data point), b) Bipolar simulation.**

The results of the analysis at the level of SFAP revealed that it can be difficult to accurately estimate CV because of end-effects. They also indicated that end-effects are dependent upon a number of fibre and measurement parameters, including relative locations of electrodes with respect to the IP and fibre terminations, and fibre depth. Further investigation was conducted at the level of multiple fibres to determine the influence of the dispersion of these parameters as a result of individual fibre differences.

### 3.3-2b The Motor Unit Action Potential

To simulate MUAPs, multiple fibres were summed. All fibre CVs were set to $v = 4\,m/s$ and the left and right termination centers were set to 120 mm and 90 mm respectively, with respect to the IZ center. To account for individual fibre differences, each fibre termination and IP location was dispersed from the center

by a value chosen uniformly between ±5 mm, and each fibre depth was dispersed from the average depth by a value chosen uniformly between ±3 mm. The dispersion limits were chosen to model a typical motor unit of the brachial biceps [106].

Figure 3-13 depicts CV estimates obtained from simulated MUAPs. Monopolar and bipolar simulations are shown at electrode locations ranging from $d = 5\,\text{mm}$ to $d = 75\,\text{mm}$, and because end-effects increase significantly as depth increases, simulations were conducted at six average depths ($r_{ave} = 5,\ 10,\ 15,\ 20,\ 25, \text{and}\ 30\,\text{mm}$). Motor units with the number of fibres increasing from $N = 1$ to $N = 200$ are shown. It is apparent from these results that for, end-effects are only evident at the extreme electrode positions ($d < 15\,\text{mm},\ \text{d} > 65\,\text{mm}$). Because CV was set to $v = 4\,\text{m/s}$ for all fibres, it was possible to calculate the root mean square error '$E_{RMS}$' of the CV estimates '$\hat{v}$' across electrode location according to:

$$E_{RMS} = \sqrt{\frac{1}{N_d}\sum_{i=1}^{N_d}\left(\hat{v}_i - v\right)^2} \qquad (3\text{-}4)$$

where $N_d$ represents the number of electrode locations.

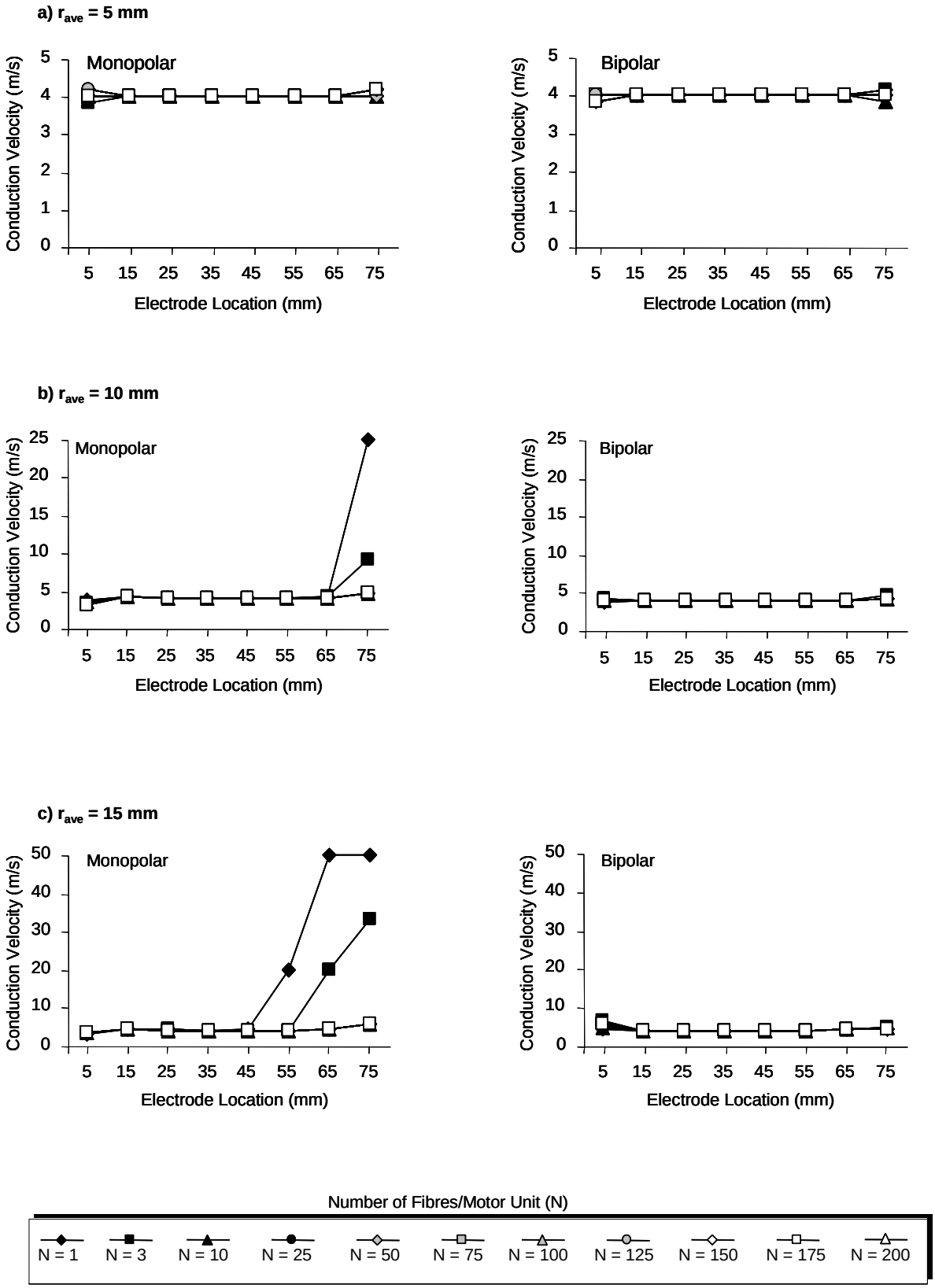


**Figure 3-13: continued on next page...**

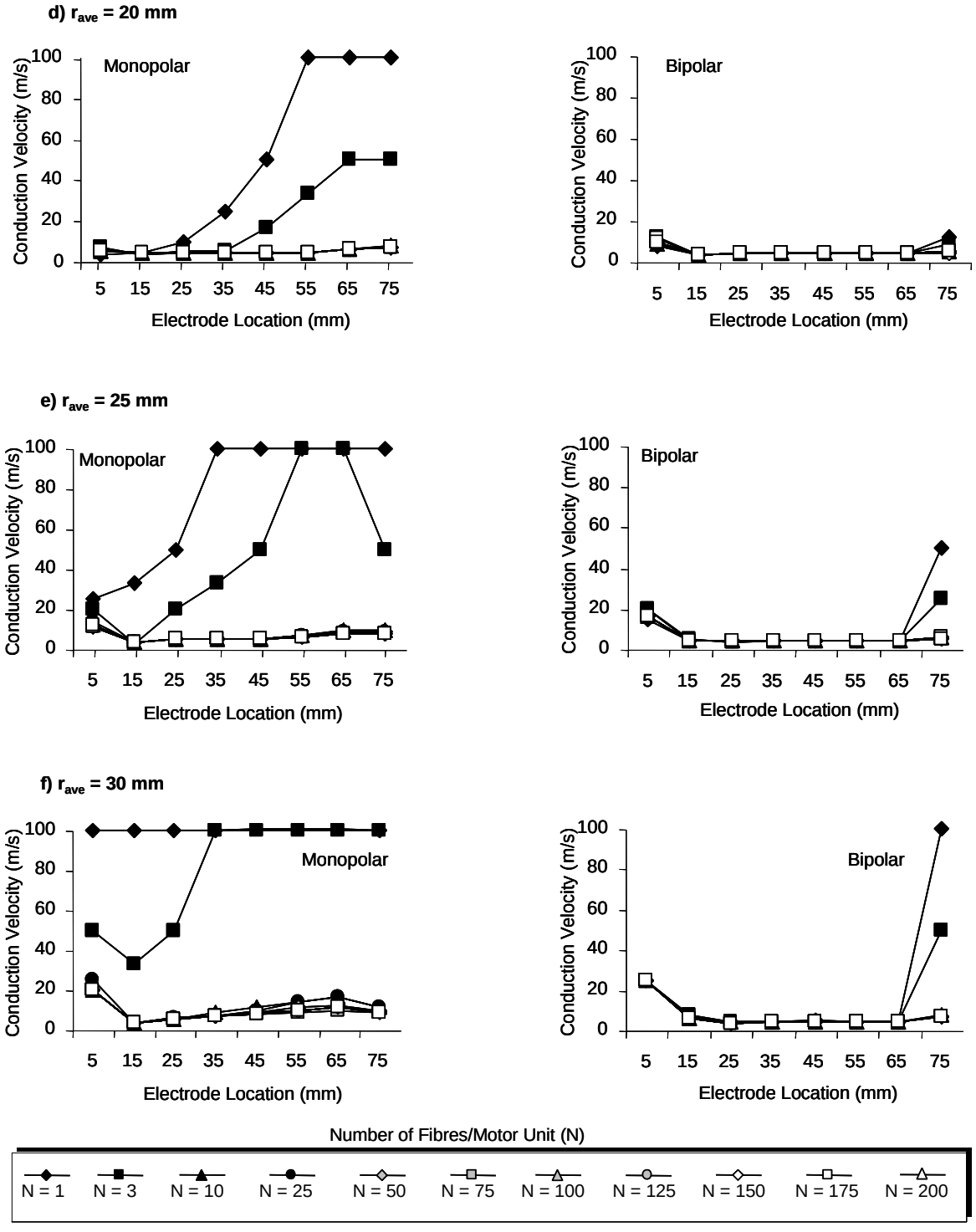


**Figure 3-13: CV estimates from simulated MUAP at various electrode locations for various numbers of fibres (s = 5 mm, $L_L$ = 120 ± 10 mm, $L_R$ = 90 ± 10 mm, r = $r_{ave}$ ± 3 mm). Monopolar and bipolar simulations are shown for a) $r_{ave}$ = 5 mm, b) $r_{ave}$ = 10 mm, c) $r_{ave}$ = 15 mm, d) $r_{ave}$ = 20 mm, e) $r_{ave}$ = 25 mm, f) $r_{ave}$ = 30 mm.**

Figure 3-14 and Figure 3-15 depict the $E_{RMS}$ values grouped by average depth. The values were split into two Figures ($N < 10$ and $N > 10$) because values from the first group were orders of magnitude larger than values from the second group (60x and 10x for monopolar and bipolar electrode configurations respectively). This indicates that dispersion in the fibre length and depth parameters attenuates the influence of end-effects on CV estimates. However, a ceiling on the attenuation effect was observed at about $N = 50$, at which point the $E_{RMS}$ values remained constant for a given depth value, regardless of the number of fibres in the motor unit.

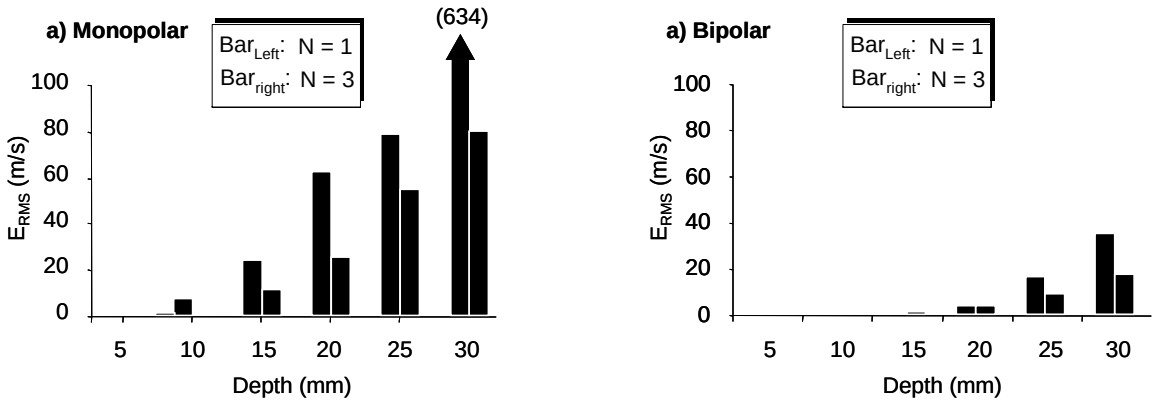


**Figure 3-14: $E_{RMS}$ of CV estimates from MUAPs with 1-3 fibres/motor unit (s = 5 mm, r = $r_{ave}$ ± 3mm, $L_L$ = 120 ± 10 mm, $L_R$ = 90 ± 10 mm, v = 4 m/s). Six average depths ($r_{ave}$) are shown from a) monopolar simulation (arrow indicates value beyond scale; actual value in brackets) and b) bipolar simulation.**

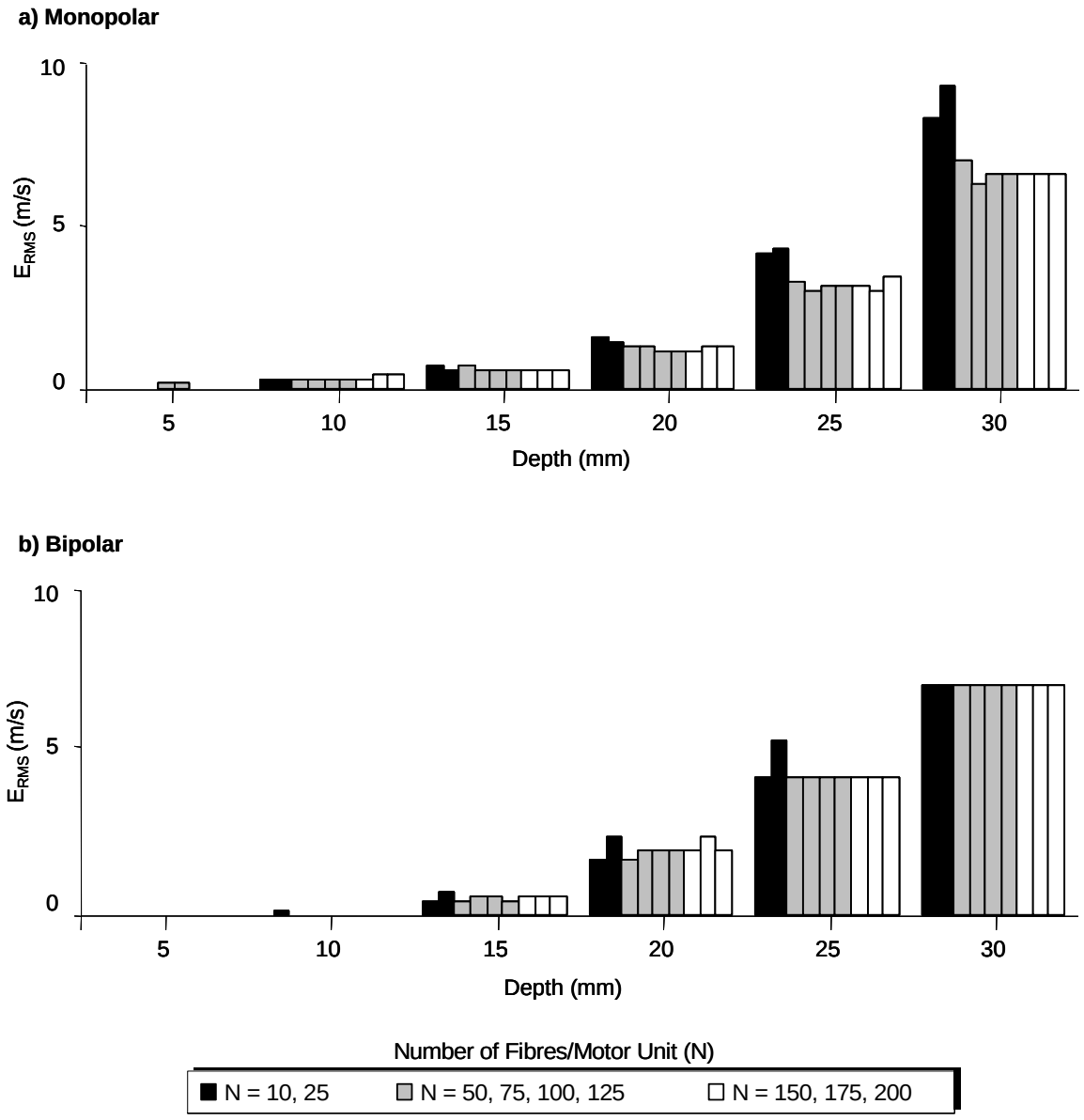


**Figure 3-15: $E_{RMS}$ of CV estimates from MUAPs with 10-200 fibres/motor unit (s = 5 mm, $L_L$ = 120 ± 10 mm, $L_R$ = 90 ± 10 mm, r = $r_{ave}$ ± 3mm). Six average depths ($r_{ave}$) are shown for a) monopolar simulation and b) bipolar simulation.**

## 3.3-2c The Myoelectric Signal

To simulate MES, MUAPs were convolved with an innervation process characterized by an independent Gaussian distribution of IPIs and the resulting MUAPts were summed. Although motor units in the brachial biceps typically

contain up to 770 fibres [12], since the previous simulation indicated no differences between motor units with $N > 50$, all MUAPs in this simulation were generated with 100 fibres. Each MUAP was generated as in the previous simulation except this time average depth '$r_{ave}$' was also dispersed. This value was randomly chosen from a uniform distribution between 5 mm and 30 mm. All MUAPts were 5 s in duration with average firing rates chosen from a Gaussian distribution ($\mu = 13/\text{s},\ \sigma = 5/\text{s}$).

Figure 3-16 depicts CV estimates obtained from the simulated MES and Figure 3-17 depicts $E_{RMS}$ values averaged across electrode location. Monopolar and bipolar electrode configurations are shown at electrode locations ranging from $d = 5\,\text{mm}$ to $d = 75\,\text{mm}$ and the number of motor units increasing from $M = 1$ to $M = 50$. Motor units were made up of $N = 100$ fibres, each with dispersion parameters described previously.

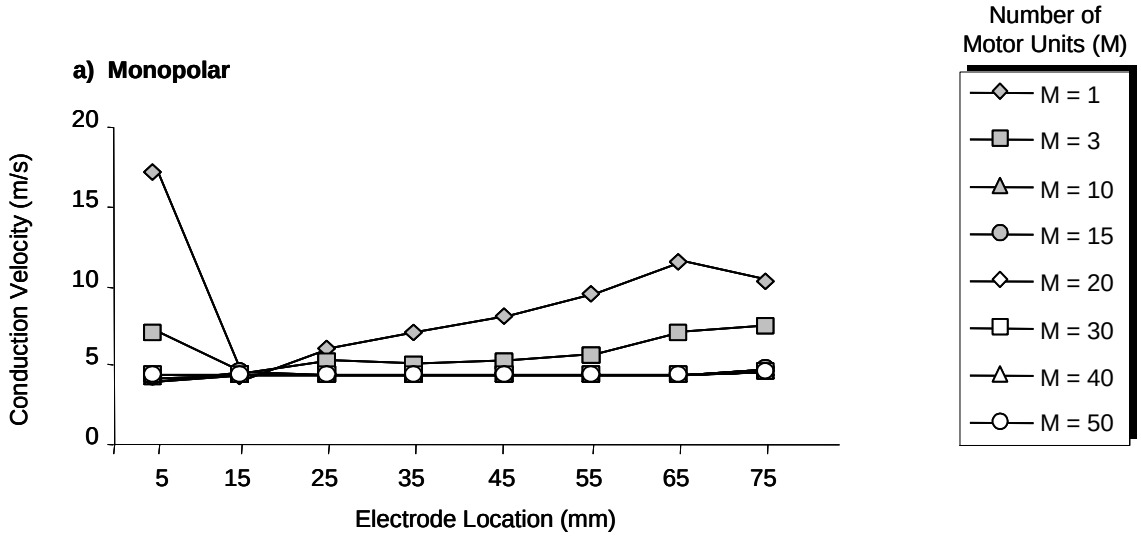


**Figure 3-16: continued on next page...**

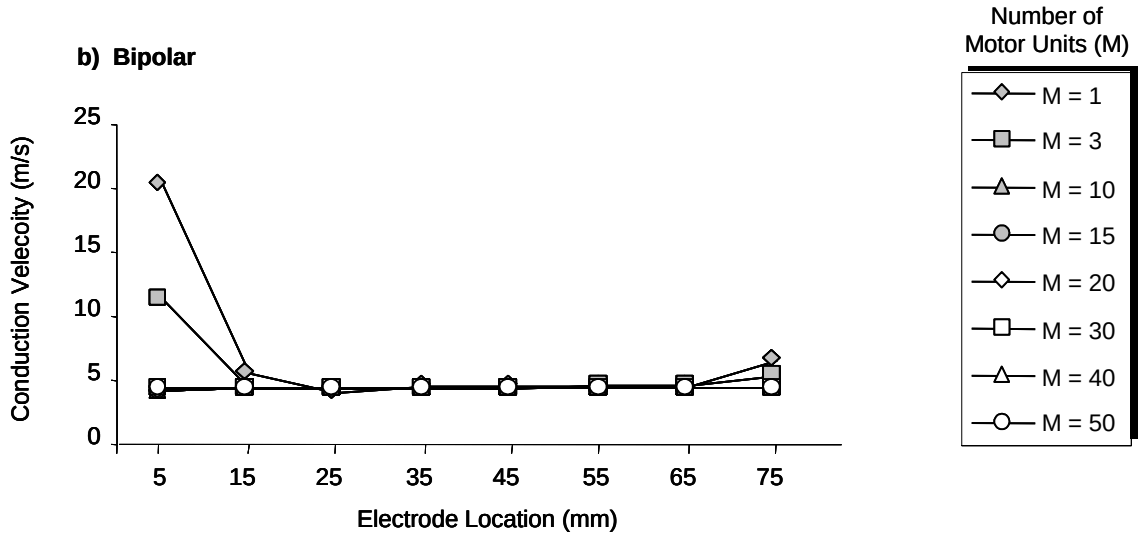


**Figure 3-16: CV estimates from simulated MES made from various numbers of motor units measured at various electrode locations (s = 5mm, $L_L = 120 \pm 10$ mm, $L_R = 90 \pm 10$ mm, $r = r_{ave} \pm 3$ mm, $r_{ave} = [5,30]$ mm, N = 100). a) Monopolar electrode configuration b) Bipolar electrode configuration.**

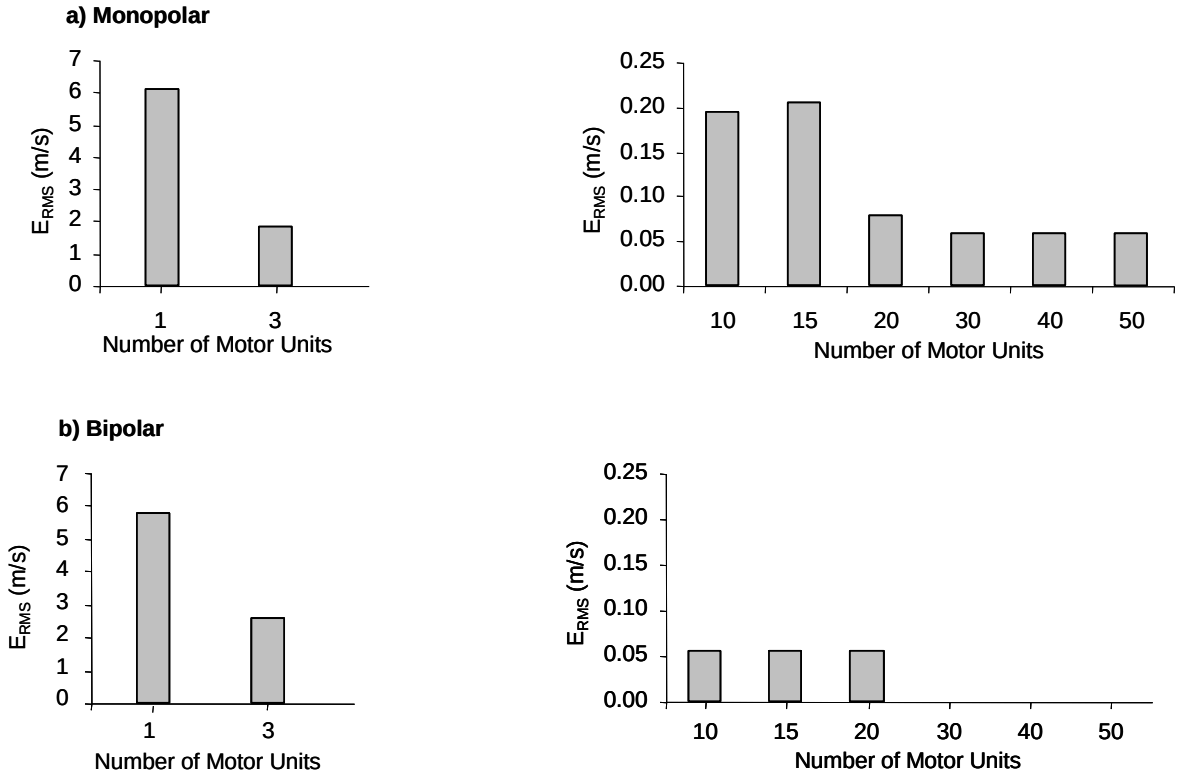


**Figure 3-17: $E_{RMS}$ of CV estimates from MES with 1-50 active motor units for a) monopolar electrode configuration and b) bipolar electrode configuration. (N = 100, s = 5 mm, $L_L = 120 \pm 10$ mm, $L_R = 90 \pm 10$ mm, $r = r_{ave} \pm 3$mm, rave = [5,30]mm).**

The results in Figure 3-16 indicate that CV estimates obtained from MES with fewer than $M = 10$ motor units may be biased, especially at extreme electrode locations ($d < 15\,\text{mm},\ d > 65\,\text{mm}$). However, this effect is depth dependent. The first 5 motor units summed in this simulation all had average depths $r_{ave} > 22\,\text{mm}$. The previous simulation indicated that CV estimates were biased at these depths. As more units were summed with depths below this limit, the bias decreased as indicated in the $E_{RMS}$ values depicted in Figure 3-17.

### 3.3-2d Summary

The SFAP simulation clearly demonstrated the existence of a non-propagating component in the SFAP due to end-effects which got larger when electrodes were placed at extreme locations and when the depth of the fibre was increased. This component of the signal manifested as a non-delay element in the cross-correlation between two channels measuring the SFAP, which caused CV estimates to be biased. This manifestation was apparent in both monopolar and bipolar measurements, although more exaggerated in the monopolar case. It was problematic for depths greater than 8 mm in the monopolar simulation and 14 mm in the bipolar simulation.

Not all fibres in a motor unit are identical and the MUAP simulation clearly demonstrated a reduction in bias due to dispersion in fibre IP locations, termination locations and depths, which eventually leveled off when more than $N = 50$ fibres were summed. While the propagating component of the MUAP

increased in amplitude with increasing fibre numbers, because the fibre length parameters were dispersed, this effect was less pronounced in the amplitude of the non-propagating component. Instead because the end-effects from each fibre did not occur at the same temporal locale in the signal, the non-propagating component spread in time as more fibres were summed. The disproportionate increase in amplitude between the propagating and non-propagating components resulted in reduced end-effects reflected in the CV measurements.

Also, since depth dispersion in a given motor unit is small compared to the depth range of the entire muscle, fibres in the motor unit are concentrated around the average fibre depth. Thus, bias was depth dependent, even in the MUAP simulation, and problematic at depths greater than 10 mm in the monopolar simulation and 15 mm in the bipolar simulation.

Finally, the MES simulation revealed that bias was reduced even further when multiple MUAPts were summed. Since an average depth was specified for each MUAPt in the MES, this reduction can be accounted for by the dispersion of average depths. Encouragingly, in the bipolar case, $E_{RMS}$ values observed at this level in the simulation were less than 0.05 m/s for $M < 20$, and non-existent for $M > 20$.

## 3.3-3 Demonstrating Electrode Misplacement Effects

There are many ways that electrodes can be misplaced when using the cross-correlation between two channels of MES to estimate CV. Not only do they have to be placed optimally to avoid end-effects, they must also be placed in alignment with the longitudinal axis of the fibres and on the same side of the IZ. While it is impossible to ensure proper alignment with all active fibres, as stated previously, choosing a small electrode spacing limits this misalignment to an acceptable level; thus, electrode misplacement effects in this context refers to the latter placement problem.

### 3.3-3a Single Fibre Analysis

As with end-effects, it is useful to examine electrode misplacement effects by observing the SFAP as measured at different electrode locations. Since results of interest occur when electrodes and/or channels straddle the IP, five electrode locations were chosen to emphasize such results. Figure 3-18 depicts the electrode locations in terms of the model parameter '$d$', which represents the distance from the IP to the first electrode in the array. In the monopolar simulation, the central point between channels was located 7.5 mm, 5 mm, 0 mm, -5 mm and -7.5 mm from the IP. The third location in this series was chosen so that the IP was evenly straddled by the monopolar channels. In the bipolar simulation, the central point between channels (which coincided with the common electrode) was located 10 mm, 2.5 mm, 0 mm, -2.5 mm, and -10 mm from the IP. The third location in this series was also chosen so that the IP was evenly straddled by the bipolar channels. Furthermore, the second and fourth

locations were chosen so that the IP was evenly straddled by the differential electrode pair making up one of the channels.

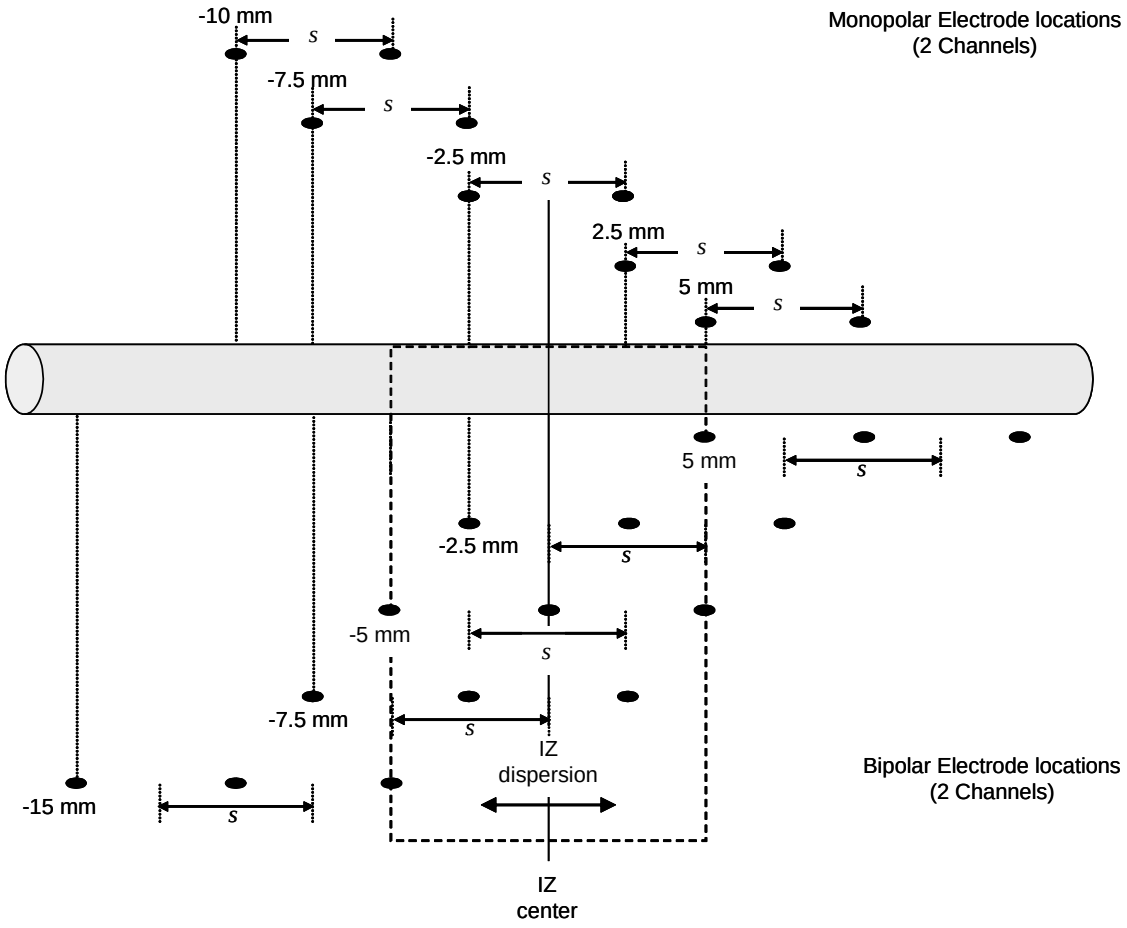


**Figure 3-18: Electrode locations for SFAP simulation demonstrating electrode misplacement effects.**

Figure 3-19 depicts the results of the monopolar simulation and Figure 3-20 depicts the results of the bipolar simulation. Two channels are illustrated and in this example $s = 5\,\text{mm}$ $L_L = 120\ \text{mm}$ , $L_R = 90\ \text{mm}$ $r = 5\,\text{mm}$, $v = 4\,\text{m/s}$ and the IP was assumed to be centered in the IZ. The depth in this example was chosen to minimize end-effects.

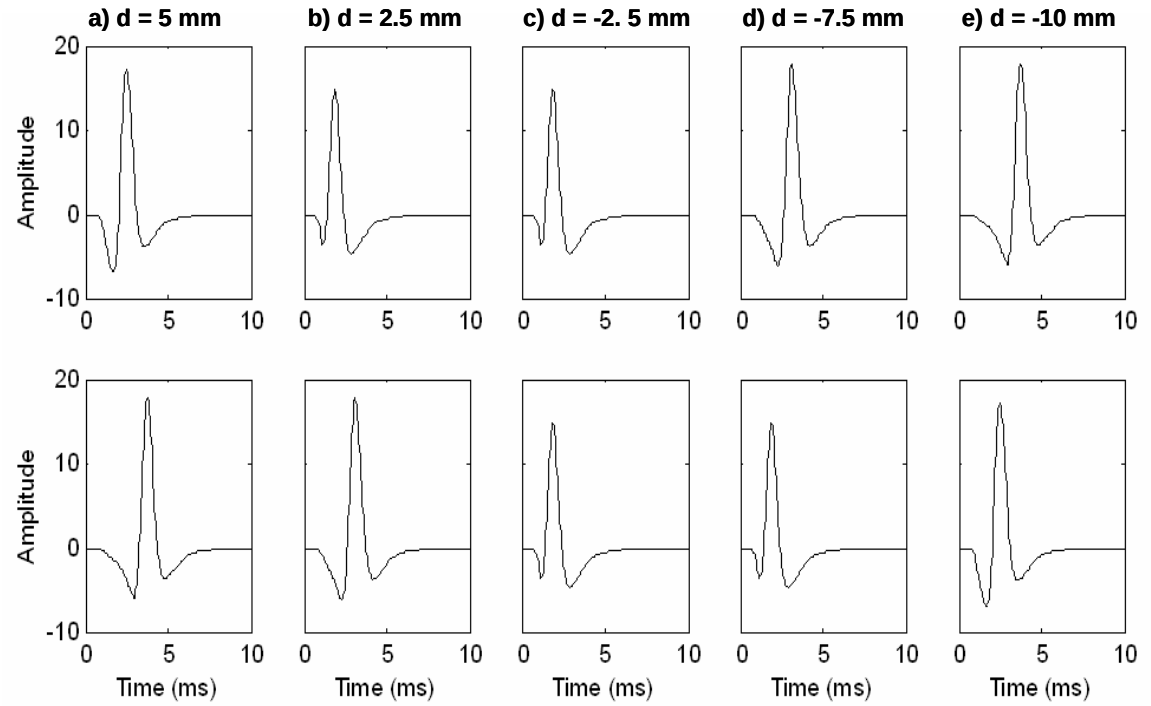


**Figure 3-19: Monopolar SFAP simulated at five electrode locations a) d = 5mm, b) d = 2.5 mm, c) d = -2.5 mm, d) d = -7.5 e) d = -10 mm. Two channels are shown (s = 5 mm, r = 5 mm, $L_L$ = 120 mm, $L_R$ = 90 mm, v = 4m/s).**

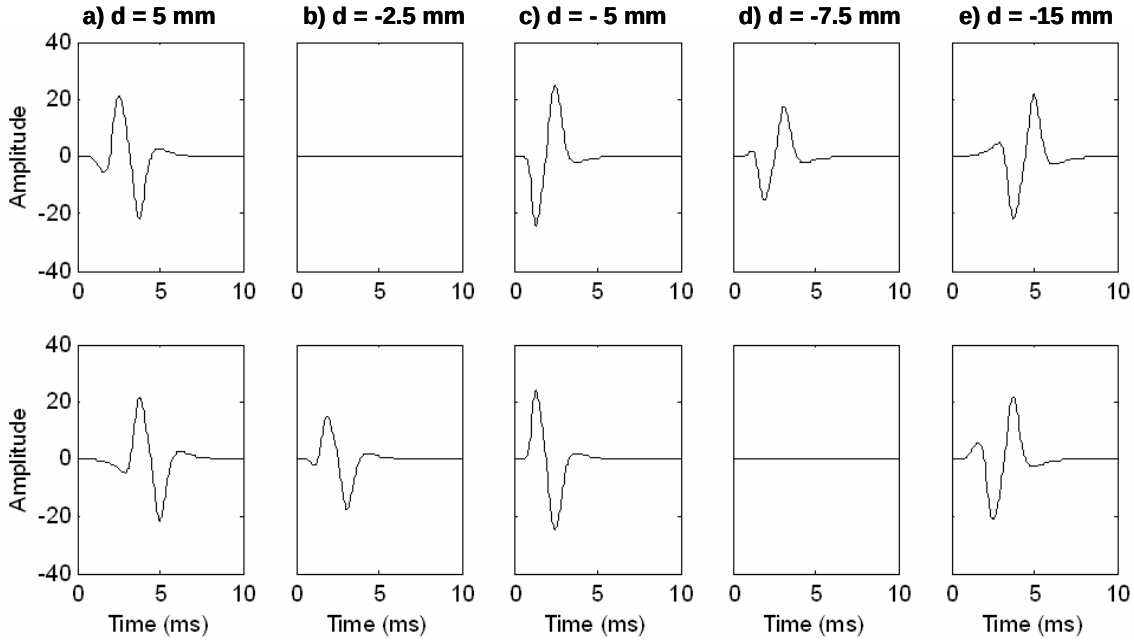


**Figure 3-20: Bipolar SFAP simulated at five electrode locations a) d = 5mm, b) d = -2.5 mm, c) d = -5 mm, d) d = -7.5 e) d = -10 mm. Two channels are shown (s = 5 mm, r = 5 mm, $L_L$ = 120 mm, $L_R$ = 90 mm, v = 4m/s).**

By visually comparing the signals from both channels at each electrode location, predictions about the cross-correlation between the channels can be made. In the monopolar simulation, at the first location, when both channels are on the same side of the IP, the signal at one channel is a shifted version of the other and the cross-correlation should be a shifted version of the autocorrelation of the signal. Mathematically, this can be demonstrated by considering a signal $s_1(t) = s(t)$ and a shifted version of that signal, $s_2(t) = s(t - \Delta)$. The time average cross correlation between $s_1(t)$ and $s_2(t)$ is given by:

$$R_{s_1 s_2}(\tau) = \frac{1}{T}\int_0^T s_1(t) \cdot s_2(t+\tau) \cdot dt \qquad (3\text{-}5)$$

$$= \frac{1}{T}\int_0^T s(t) \cdot s(t - \Delta + \tau) \cdot dt$$

$$= R_{ss}(\tau - \Delta)$$

At the second location, both monopolar channels are still on the same side of the IP so the cross-correlation should be similar to that of the first instance. At the third location, the monopolar channels are evenly straddling the IP. This causes identical signals to arrive at each electrode at exactly the same time; thus the cross-correlation should be a non-shifted version of the autocorrelation. Each of these predictions is confirmed in Figure 3-21.

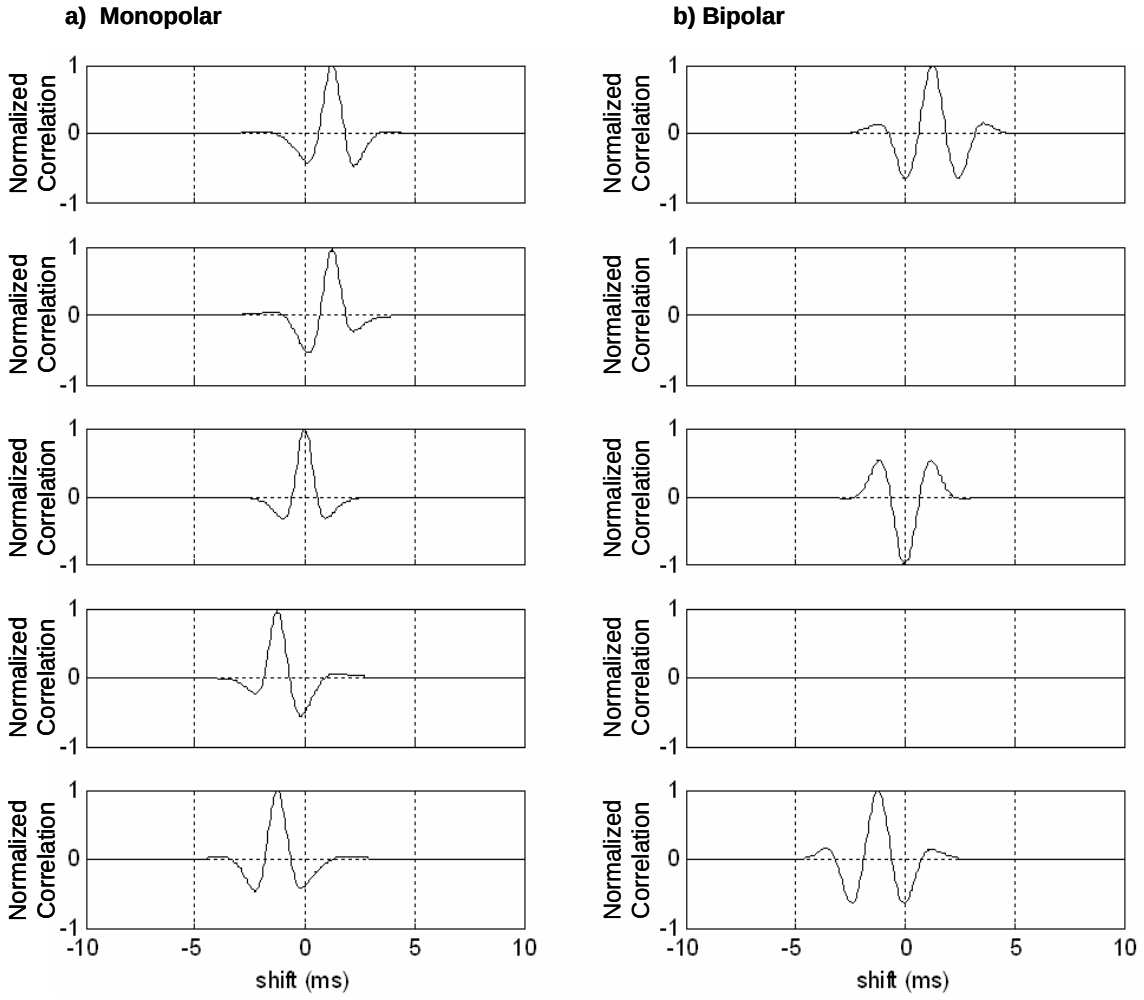


**Figure 3-21: Cross-correlation between simulated SFAP from two channels at five electrode locations (s = 5 mm, r = 5 mm, $L_L$ = 120 mm, $L_R$ = 90 mm, v = 4m/s). a) Monopolar simulation (d = 5mm, 2.5 mm, d = -2.5 mm, d = -7.5 d = -10 mm) b) Bipolar simulation (d = 5mm, -2.5 mm, d = -5 mm, d = -7.5 d = -15 mm).**

At the last two locations, both monopolar channels have passed the IP and are again on the same side. These locations are identical to the first two, except that the second channel is now closer to the IP than the first. Thus, the cross-correlations should be identical to the cross-correlations in the first two instances except that the shift should be in the opposite direction, as indicated in Figure 3-21.

In the bipolar simulation, because each channel is a differential pair, further considerations must be made. At the first location, both channels are on the same side of the IP, so the signal at one channel is a shifted version of the other and the cross-correlation should be a shifted version of the autocorrelation of the signal. However, at the second location, one of the differential pairs straddles the IP. Since the signal at one electrode is identical to the signal at the other electrode in this channel, the resulting bipolar signal is zero. The other differential pair records a signal because both electrodes in this channel are on the same side of the IP. Thus, the cross-correlation between channels is completely degraded.

At the third location, the bipolar channels perfectly straddle the IP. Thus, on the left side of the IP the bipolar signal is calculated according to:

$$x_{BP_{LS}}(t) = x_{MP_1}(t) - x_{MP_2}(t) \qquad (3\text{-}6)$$

while the signal on the right side is calculated according to:

$$x_{BP_{RS}}(t) = x_{MP_2}(t) - x_{MP_3}(t) \qquad (3\text{-}7)$$

Since $x_{MP_2}(t)$ is common to both channels, and $x_{MP_1}(t) = x_{MP_3}(t)$ at this location, the bipolar signals are equal and opposite and the cross-correlation should be the negative of the autocorrelation. The last two locations are identical to the first two, except that the electrodes in each differential pair are reversed because the

channels have moved to the other side of the IP. Thus, the bipolar signals at these locations are negatives to those in the first two instances and the cross-correlations should be identical except that the delay should be in the opposite direction. Figure 3-21 confirms all of these predictions.

It is apparent from the SFAP analysis that electrode misplacement effects can have a profound influence on CV estimates. At the extreme, when the channels evenly straddle the IP, there is no delay in the cross-correlation and CV estimation approaches infinity. Furthermore, in the bipolar configuration, when one channel straddles the IP, the correlation between channels degrades to zero. Thus it can be difficult to estimate CV when the location of the innervation point is uncertain. To determine the influence of dispersion of IPs amoung fibres, further investigation was conducted at the level of multiple fibres.

### 3.3-3b Multiple Fibre Analysis

According to the multiple fibre analysis on end-effects, even at locations close to the innervation zone, end-effects were negligible in MES with the number of motor units $M > 30$ when each motor unit was made up of at least 100 fibres. To avoid end-effects while observing electrode misplacement effects, a simulation within these constraints was conducted.

MES was simulated by summing $M = 50$ motor units made up of $N = 100$ fibres and convolved with an innervation process as previously described. All fibre CVs were set to $v = 4\,\mathrm{m/s}$ and the left and right termination centres were set to 120

mm and 90 mm respectively, with respect to the IZ center. To account for individual fibre differences, each fibre termination and IP location was dispersed from the center by a value chosen uniformly between ±5 mm, and each fibre depth was dispersed from the average depth by a value chosen uniformly between ±3 mm. Finally, the average depth of each motor units was chosen from a uniform distribution between 5 mm and 30 mm. Figure 3-22 depicts the results for the electrode locations defined in the single fibre analysis.

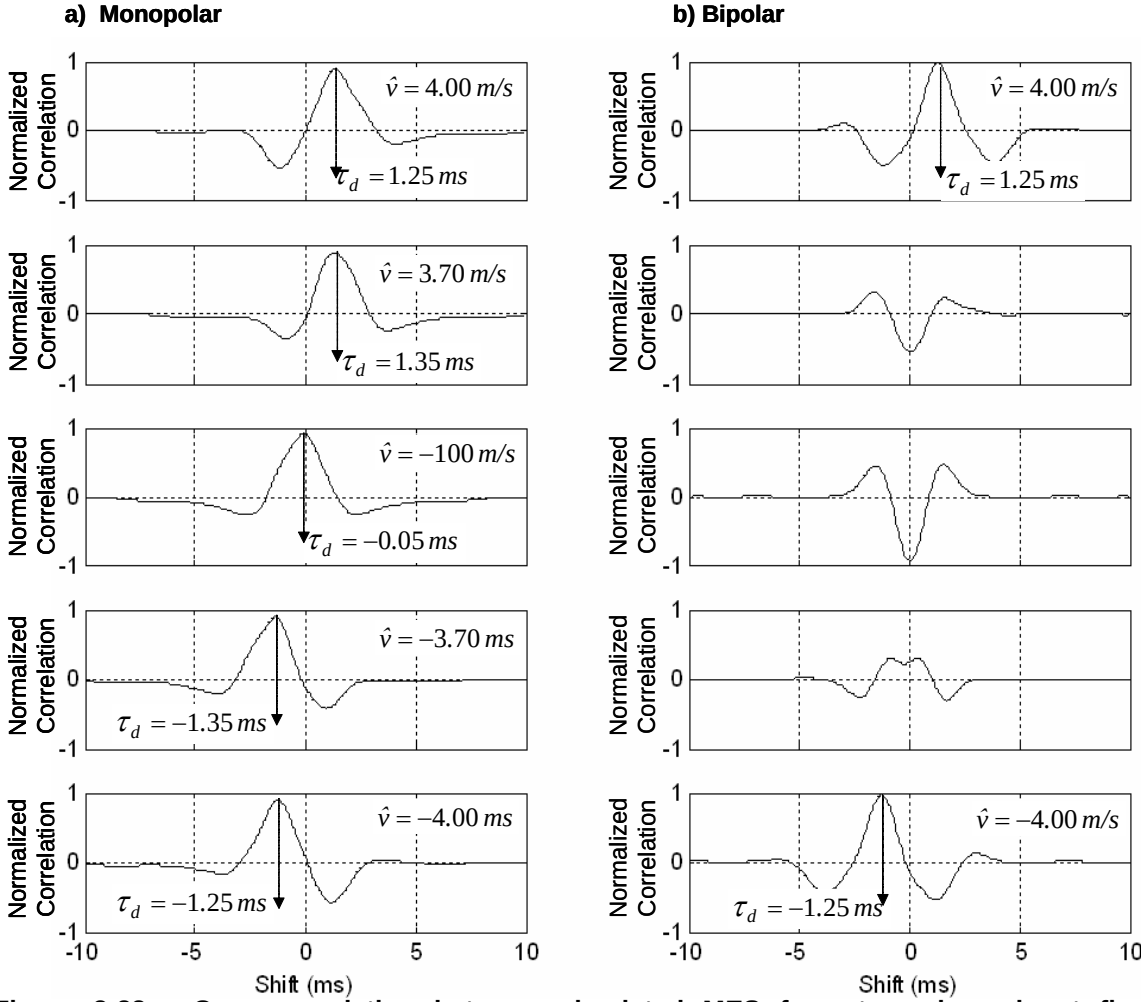


**Figure 3-22: Cross-correlation between simulated MES from two channels at five electrode locations (s = 5 mm, r = 5 mm, $L_L$ = 120 mm, $L_R$ = 90 mm, v = 4m/s). a) Monopolar simulation (d = 5mm, 2.5 mm, d = -2.5 mm, d = -7.5 d = -10 mm) b) Bipolar simulation (d = 5mm, d = -2.5 mm, d = -5 mm, d = -7.5 d = -15 mm).**

Because of the dispersion of parameters, results from the multiple fibre analysis were not as predictable compared with the single fibre analysis. Nevertheless, similar trends exist. At the first and last electrode locations, all the electrodes in the array were on one side of the IZ and an accurate estimate of CV was obtainable. At the inner three locations, one or more electrodes in the array were contained within the IZ, yielding cross-correlations from which a reasonable CV estimate was not possible to ascertain.

### 3.3-4 Modeling End-effects and Electrode Misplacement Effects caused by changes in Dynamic Factors

As confirmed in the previous simulations, electrode position is a critical factor in meeting the assumptions required to obtain reasonable CV estimates. End-effects, which manifest as non-propagating components in MES, can introduce a non-delay element into the cross-correlation which biases the CV estimate. These effects increase as depth of active muscle fibres increases and as electrodes get closer to the innervation zone or fibre termination regions. Also, effects have been shown on the cross-correlation which increase the variability of CV estimates as electrodes traverse the innervation zone.

As joint angle decreases, muscle fibre length decreases and the innervation zone may migrate towards the measuring electrodes. If substantial, these changes could cause increased bias and/or variability in CV estimations. Simulated MES was generated to determine the possible influence of end-effects and innervation

zone migration leading to electrode misplacement effects on CV estimates obtained at different joint angles.

MES as generated previously was simulated with $M = 50$, $N = 450$. All fiber CVs were set to $v = 4\ \mathrm{m/s}$, IP and termination dispersions were set to $\pm$5 mm, MUAP depth dispersions were set to $\pm$ 3 mm and the average depth of a given motor unit was chosen randomly from a uniform distribution between 5 mm and 30 mm. During this simulation however, the left and right termination centers were located at seven progressively shorter distances from the IZ center in order to model the effects of shortening muscle fibers ($L_L, L_R = 120 \pm 5,\ 110 \pm 5,\ 100 \pm 5,\ 90 \pm 5,\ 80 \pm 5,\ 70 \pm 5,\ 60 \pm 5\ \mathrm{mm}$).

Two simulations were conducted. First, the electrode array was optimally located with the first electrode placed at $d = 35\ \mathrm{mm}$. An extra electrode was included so that a double differential measurement could also be simulated. Figure 3-23 depicts the results of this simulation. Then the simulation was repeated but at each progressive length change, the IZ center was shifted 8 mm towards the right termination, iteratively decreasing the distance between the IZ center and the electrode location ($d = 35,\ 27,\ 19,\ 11,\ 3,\ -5,\ -13\ \mathrm{mm}$). Figure 3-24 depicts these results.

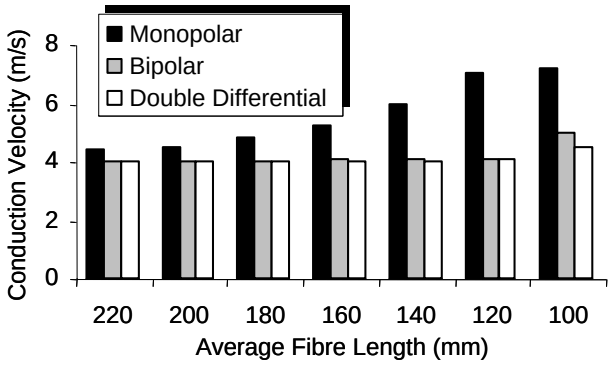


**Figure 3-23: CV estimates from simulated MES with 50 active motor units with N = 100 fibres/motor unit at seven average fiber lengths ($L_L$, $L_R$ = 110 ± 5 mm, 100 ± 5 mm, 90 ± 5 mm, 80 ± 5 mm, 70 ± 5 mm, 60 ± 5 mm, 50 ± 5 mm) for monopolar (■), bipolar (■), and double differential (□) electrode configurations. (d = 35 mm, s = 5 mm, r = $r_{ave}$ ± 3mm, rave = [5,30]mm).**

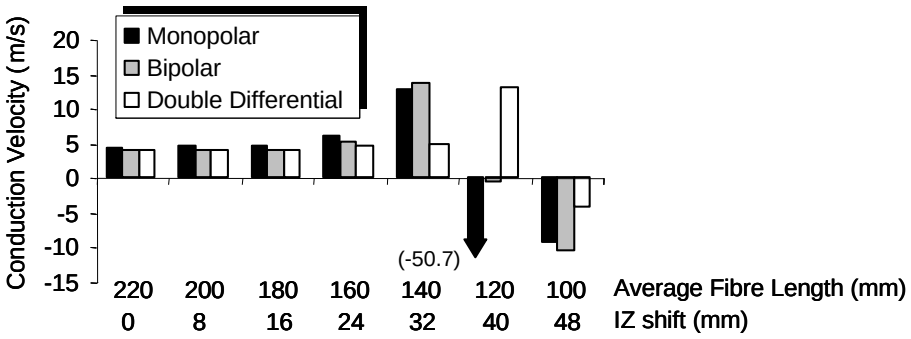


**Figure 3-24 CV estimates from simulated MES with 50 active motor units with N = 100 fibres/motor unit at seven average fiber lengths ($L_L$, $L_R$ = 110 ± 5 mm, 100 ± 5 mm, 90 ± 5 mm, 80 ± 5 mm, 70 ± 5 mm, 60 ± 5 mm, 50 ± 5 mm) while IZ is shifting (d = 35 mm, 27 mm, 19 mm,11 mm, 3 mm, -5 mm, -13 mm) for monopolar (■), bipolar (■), and double differential (□) electrode configurations. (s = 5 mm, r = $r_{ave}$ ± 3mm, rave = [5,30]mm).**

According to the results of the first simulation, while bias in the monopolar estimation gets increasingly worse, in the bipolar simulation the estimate does not begin to be substantially biased until the average fibre length has shortened

by about 55% (from 220 mm to 100 mm), and even then, the bias in the bipolar estimate ($\hat{v}_{BIAS} = 1\,\text{m/s}$) is much smaller than the bias in the monopolar estimate ($\hat{v}_{BIAS} = 3.2\,\text{m/s}$). In the double differential estimate, this observation is even more pronounced ($\hat{v}_{BIAS} = 0.5\,\text{m/s}$). Since expected muscle shortening is typically not greater than 25% [108], at least in the brachial biceps (see appendix B for biomechanical model), these results are encouraging.

The results of the second simulation are not as encouraging. The bias in both the monopolar and bipolar estimates begins to be substantial when the innervation zone gets within 3 mm of the electrode array, and while it passes through the array the estimates get worse. While these effects are delayed in the double differential estimate, they are still apparent at the 6$^{th}$ iteration, when the IZ was aligned with the electrode array.

The results of this investigation indicate that end-effects due to muscle fibres shortening with joint angle can probably be controlled sufficiently with a double differential electrode configuration and careful electrode placement. However, the effects of electrode misplacement due to innervation zone migration may be problematic. Therefore, further investigation was warranted to determine whether or not the IZ actually migrates as joint angle changes.

## 3.4 INNERVATION ZONE MIGRATION WITH CHANGES IN JOINT ANGLE – EXPERIMENT 2

### 3.4-1 Purpose

The purpose of this experiment was to determine the extent to which IZ migrates with changes in joint angle. Data were collected from the brachial biceps with the elbow held at five joint angles. An IZ location was determined for each joint angle by comparing channels of MES collected simultaneously at distributed locations along the length of the muscle using an eight channel electrode array.

### 3.4-2 Method

Data were collected from five participants for this experiment – three females aged 35, 28, and 27 respectively, and two males aged 22, 25 respectively. The brachial biceps in the dominant arm was the muscle of interest. The central pulley apparatus as described in Section 3.2-2 was also used in this experiment to monitor elbow joint angle and control load.

Using the apparatus in fastened mode, an MVC measurement was taken for each participant with joint angle fixed at 50°, 70°, 90°, 110°, and 130° respectively. One day after the MVC tests, participants returned for signal acquisition. Using the central pulley apparatus, participants were instructed to hold the disc at 50°, 70°, 90°, 110°, and 130° against loads equivalent to 20% of their MVCs. Each angle was held for 5 s and a one minute rest interval between

each combination was imposed. The order in which participants held the five joint angles was randomized.

MES was recorded using a bar electrode array with eight 0.5 mm x 10 mm bars permanently fixed 10.0 mm apart. The bars were configured in single differential mode yielding seven channels with an effective separation of 10.0 mm. Before electrodes were placed, the skin surface on which the array was mounted was cleansed with rubbing alcohol and treated with conducting gel. The array was placed along the short head of the muscle such that the most proximal electrode was 150 mm below the access point of the clavicle into the shoulder joint.

All MES channels were processed identically through the acquisition instrumentation as described in Section 3.2-2, except the sampling rate for analogue to digital conversion was set to $f_s = 1024$ Hz. In total, five sets of data records were obtained for each participant; one set of seven channels for each angle. Plots of each of the data sets were visually inspected. When the electrode array traversed the IZ, a reversal in propagation direction was observed amoung the channels and the IZ was assumed to be located between the channels at which the reversal occurred.

### 3.4-3 Results

Table 3-3 lists the MVC results obtained for each of the five participants in this experiment:

| Angle | P1 | P2 | P3 | P4 | P5 |
|---|---|---|---|---|---|
| **50°** | 11.24 kg | 13.47 kg | 7.98 kg | 21.05 kg | 24.82 kg |
| **(20% MVC)** | (2.25 kg) | (2.69 kg) | (1.59 kg) | (4.21 kg) | (4.96 kg) |
| **70°** | 11.61 kg | 13.84 kg | 7.43 kg | 22.43 kg | 24.82 kg |
| **(20% MVC)** | (2.32 kg) | (2.76 kg) | (1.48 kg) | (4.48 kg) | (4.96 kg) |
| **90°** | 11.61 kg | 13.10 kg | 7.98 kg | 22.43 kg | 24.82 kg |
| **(20% MVC)** | (2.32 kg) | (2.62 kg) | (1.59 kg) | (4.48 kg) | (4.96 kg) |
| **110°** | 10.12 kg | 12.73 kg | 7.70 kg | 19.00 kg | 22.36 kg |
| **(20% MVC)** | (2.02 kg) | (2.54 kg) | (1.54 kg) | (3.80 kg) | (4.47 kg) |
| **130°** | 9.38 kg | 11.61kg | 6.88 kg | 18.04 kg | 20.91 kg |
| **(20% MVC)** | (1.87 kg) | (2.32 kg) | (1.37 kg) | (3.61 kg) | (4.18 kg) |

**Table 3-3: MVC Results from Experiment 2**

Figures 3-25 to 3-29 depict a segment of data at each of the angles for all five participants. A reversal in propagation direction is clearly observable at all of the joint angles in Figure 3-25, Figure 3-26 and Figure 3-28. These figures refer to participants 1, 2 and 4 respectively. The shaded area in each plot represents the region in which the reversal occurs and the IZ is assumed to be located within this region. For all three cases, a proximal migration of this region is evident as joint angle decreases. Figure 3-30 depicts a plot of IZ location vs joint angle for each of these participants, based upon the regions outlined.

The data collected from participants 3 and 5 as depicted in Figure 3-27 and Figure 3-29 were less discernable. In both cases it was impossible to determine a propagation direction at any angle because the correlation between many channels was too low, and when correlation was sufficiently high almost no shift in either direction could be detected.

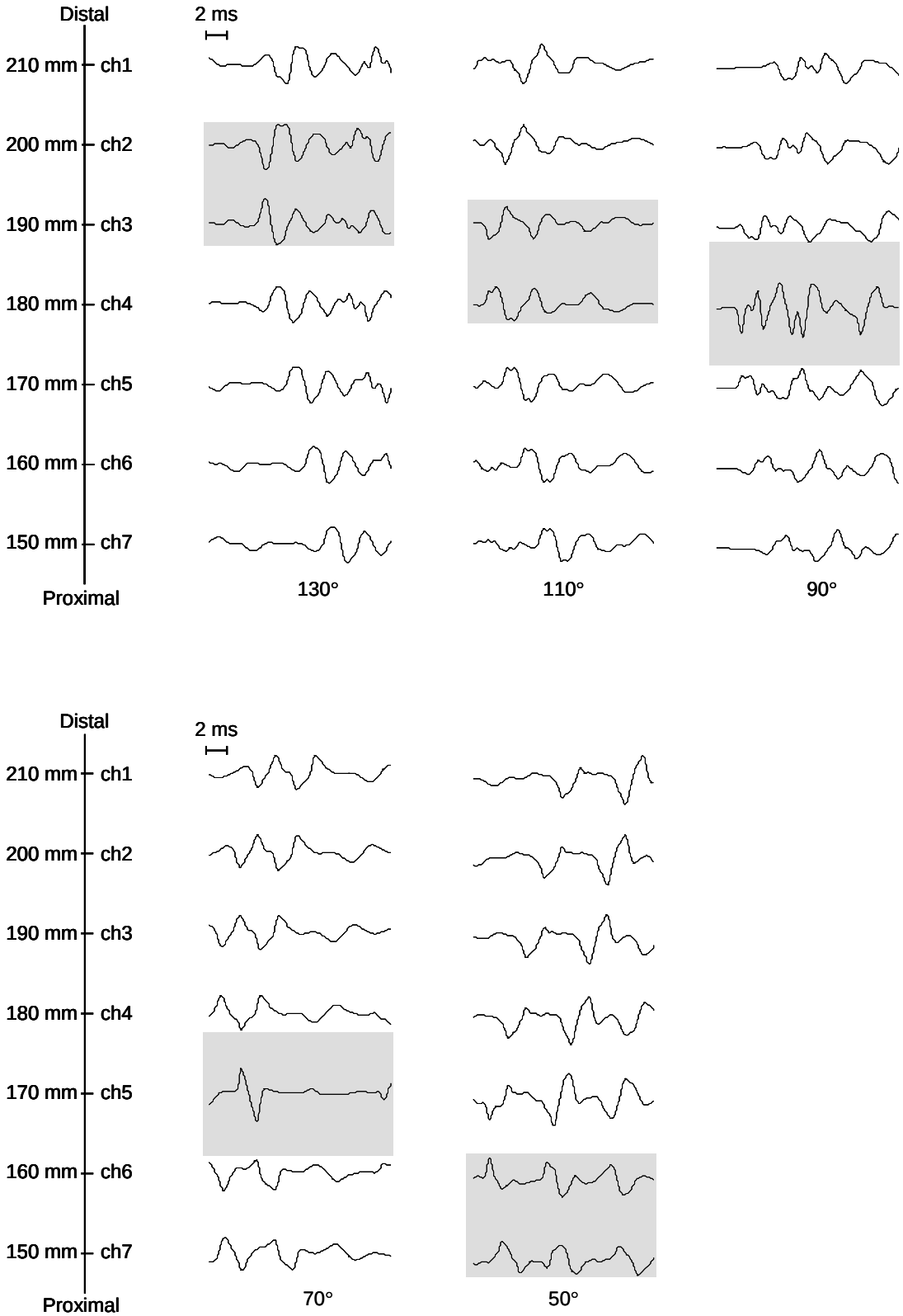


**Figure 3-25: Segments of MES collected from seven channels at five joint angles for participant 1 in experiment 2. Distances are measured from the access point of the clavicle to the shoulder joint. Shaded areas represent the region in which IZ resides.**

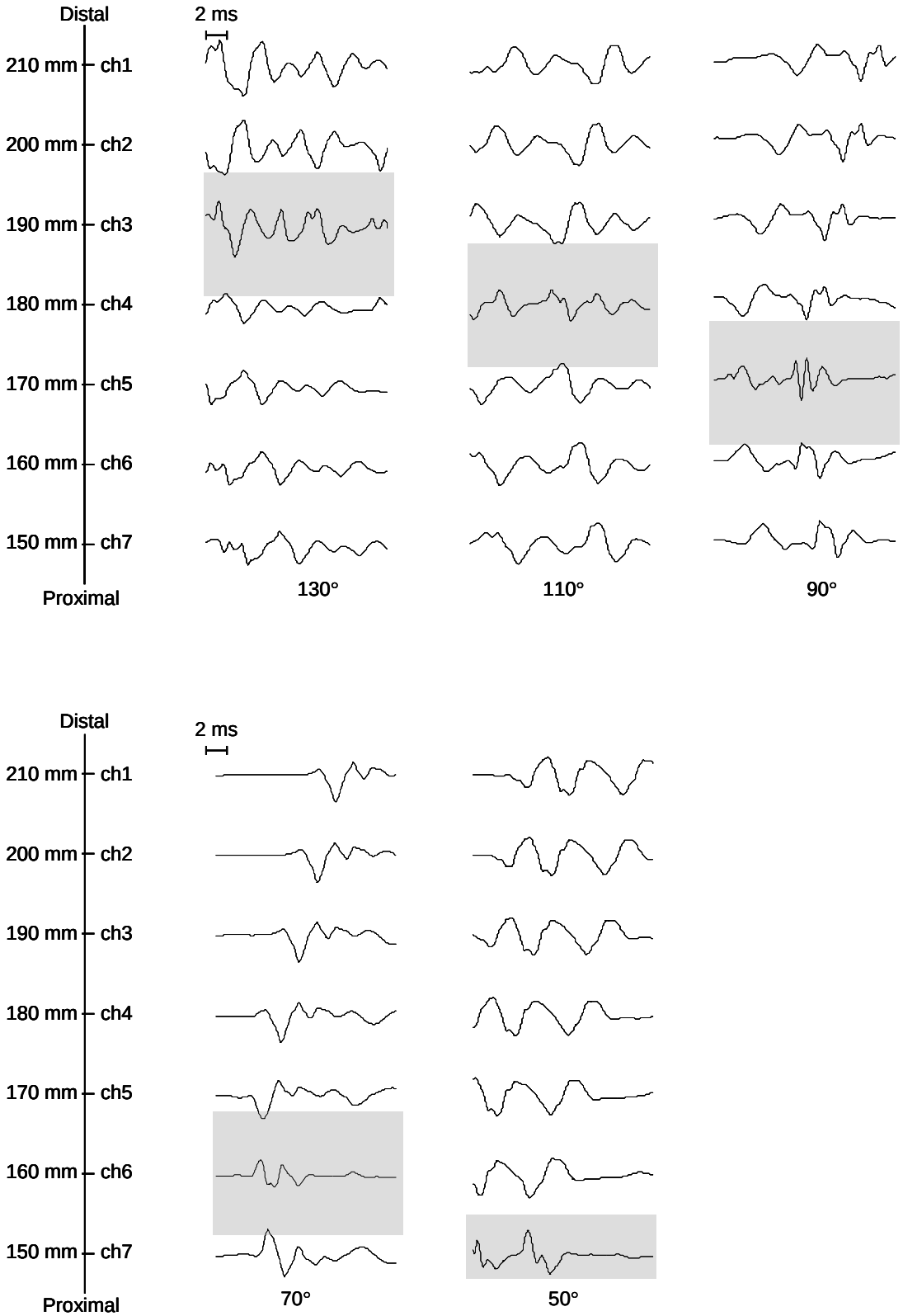


**Figure 3-26: Segments of MES collected from seven channels at five joint angles for participant 2 in experiment 2. Distances are measured from the access point of the clavicle to the shoulder joint. Shaded areas represent the region in which IZ resides.**

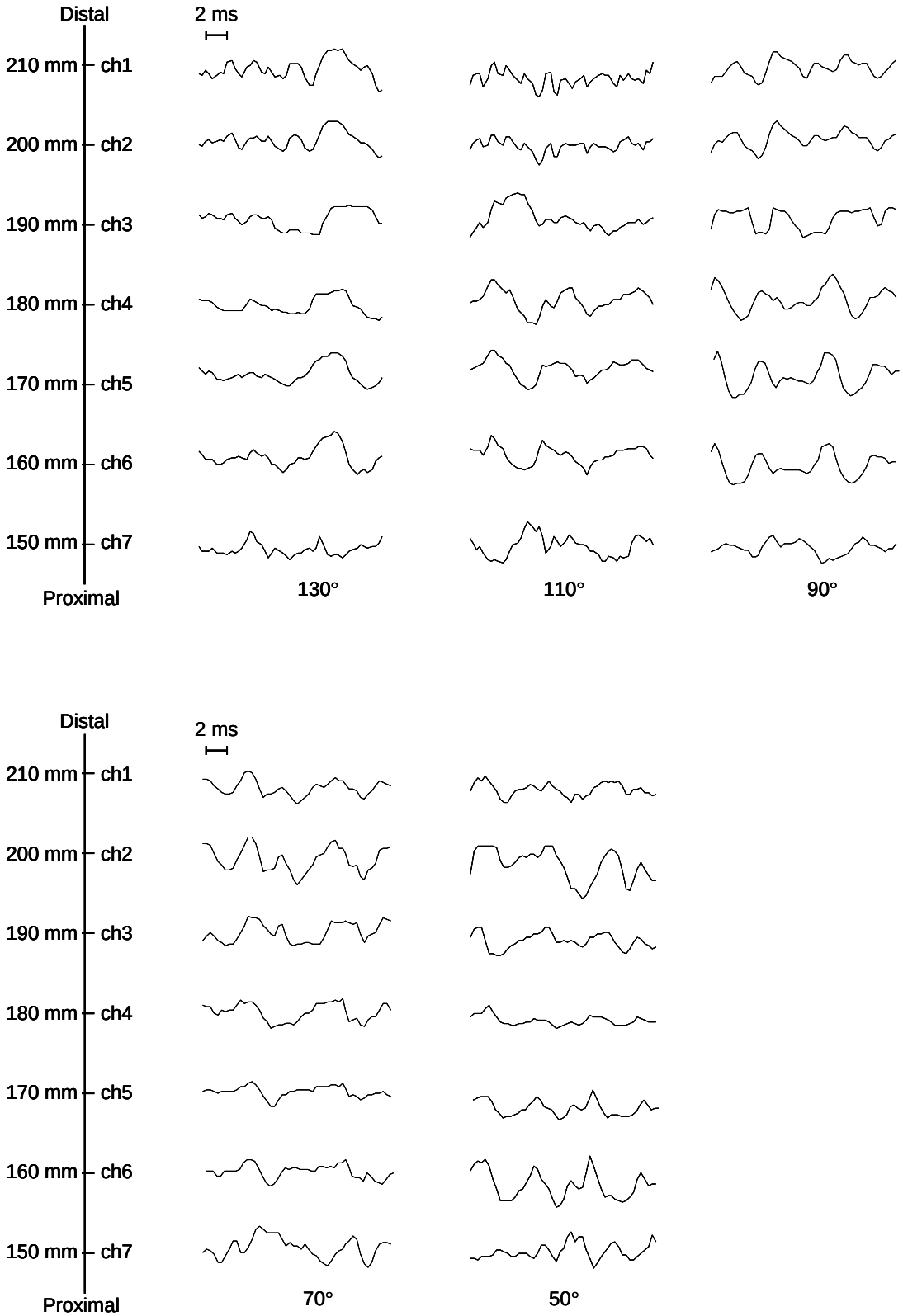


**Figure 3-27: Segments of MES collected from seven channels at five joint angles for participant 3 in experiment 2. Distances are measured from the access point of the clavicle to the shoulder joint. Shaded areas represent the region in which IZ resides.**

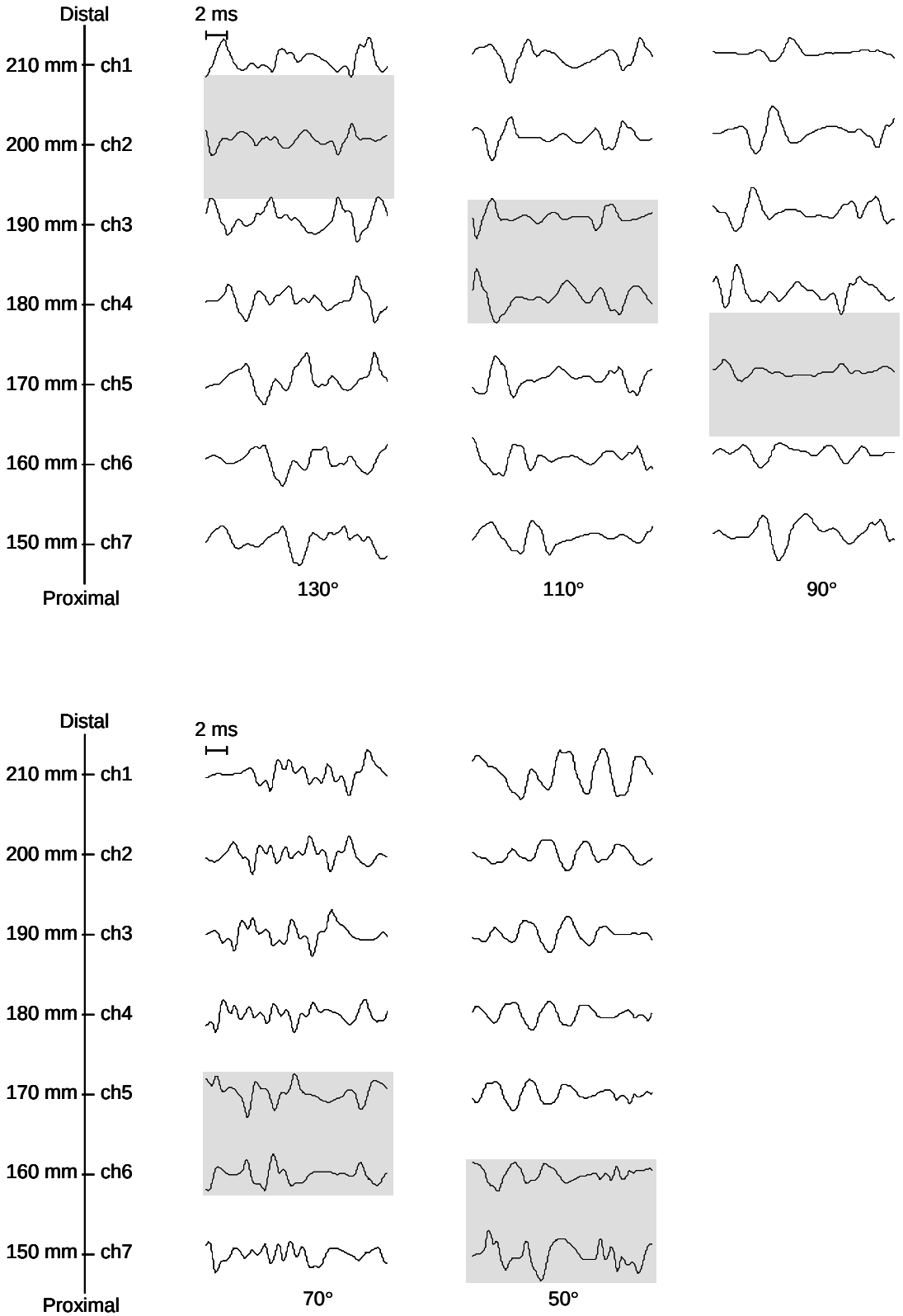


**Figure 3-28: Segments of MES collected from seven channels at five joint angles for participant 4 in experiment 2. Distances are measured from the access point of the clavicle to the shoulder joint. Shaded areas represent the region in which IZ resides.**

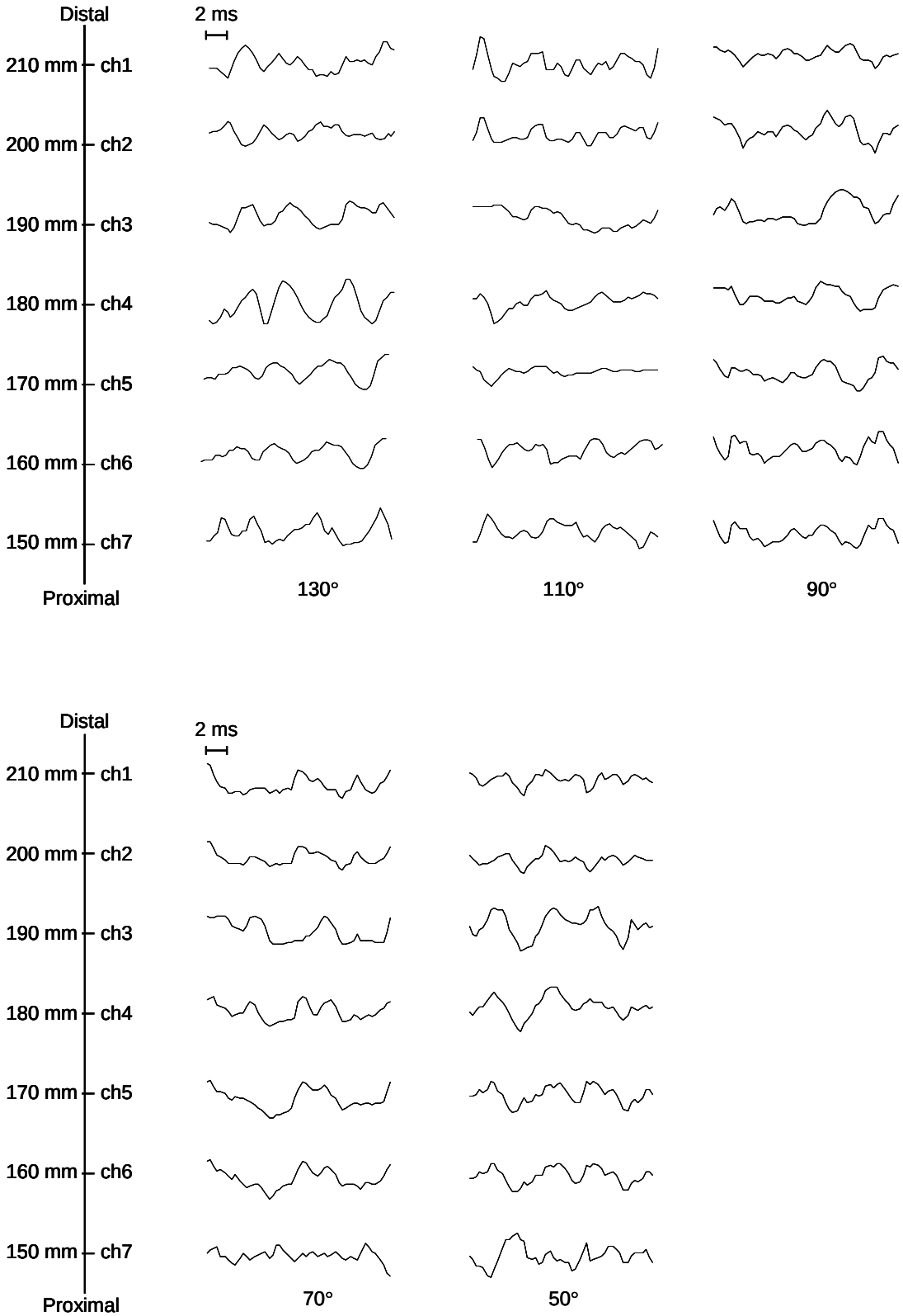


**Figure 3-29: Segments of MES collected from seven channels at five joint angles for participant 5 in experiment 2. Distances are measured from the access point of the clavicle to the shoulder joint. Shaded areas represent the region in which IZ resides.**

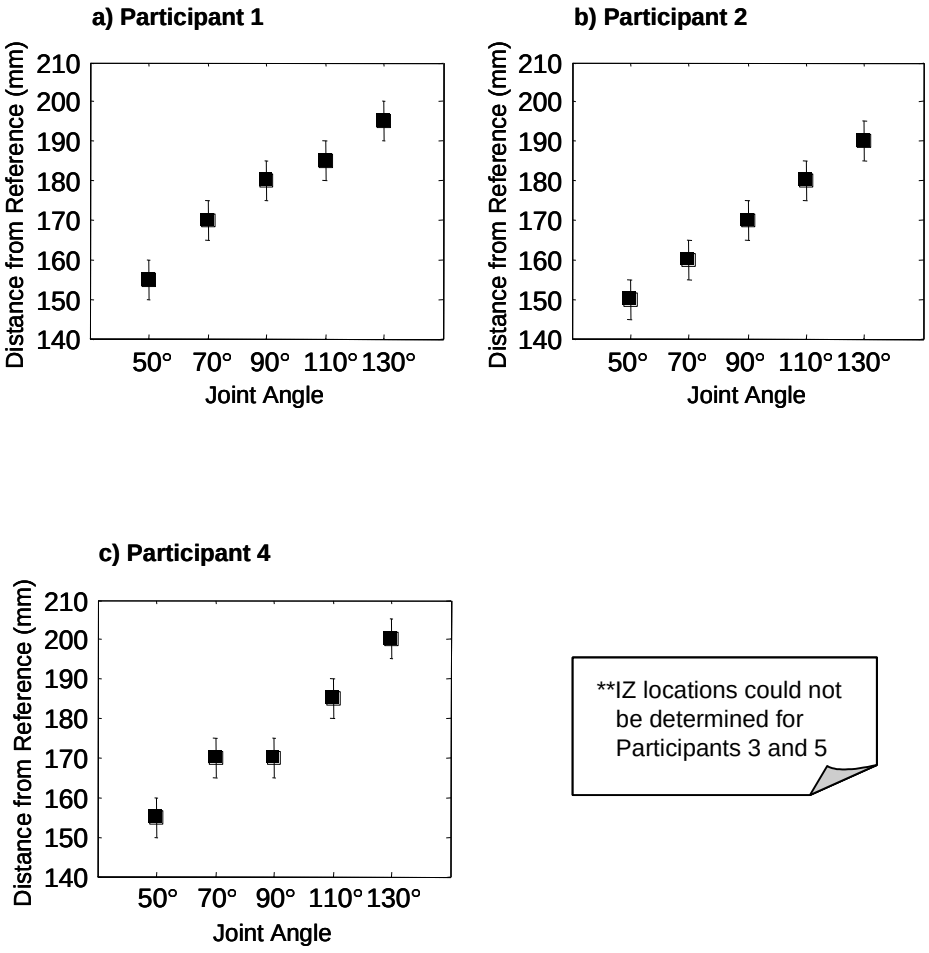


**Figure 3-30: IZ location vs joint angle from experiment 2 for all participants for which IZ location was observable based upon reversal of propagation direction. Error bars represent the range in which IZ resides.**

## 3.4-4 Explanation of Results

As indicated in Figures 3-25 to 3-29, three of the five participants in this experiment demonstrated an IZ migration with joint angle. While spatial resolution limited the precision of the migration measurements, the migration was at least 30 mm in all three cases.

It was not possible to determine IZ location at any angle for two of the participants in this experiment since the correlations between channels was often low and propagating components could not be observed. Since these findings were observed at all joint angles and throughout all channels in the array, end effects are an unlikely cause. In some instances, the difference in signals could be attributed to channels traversing the IZ. However, it is improbable that one IZ would occupy the entire length of the electrode array. Perhaps participants 2 and 5 were endowed with two IZs, an observation not uncommon in the brachial biceps [10, 12, 13]. Another viable explanation is that the electrode array was misaligned with too many of the fibres within the muscle because of improper placement. While care was taken to ensure that the array was placed in proper alignment, the two-headed nature of the brachial biceps can make this a difficult task. Regardless of the reason for the unwieldy results, they exemplify the problematic nature associated with obtaining accurate CV estimates.

### 3.4-5 Conclusion

According to the results of this experiment, location of the IZ is affected by joint angle, enough to make CV estimation with a single pair of bar electrode channels problematic. The range of migration found within this experiment suggests that it may be possible to pre-analyze the muscle of interest to find an electrode location which satisfies the requirements for all joint angles, but a more efficient approach may be to use an electrode array together with some gating algorithm which specifies an appropriate subset of channels to utilize based on some post-

processing criteria. While such a technique may be promising, the troublesome data sets also collected in this experiment suggest cautious optimism with regard to accurate CV estimation.

## SUMMARY OF CONDUCTION VELOCITY EXAMINATION

Power spectral parameters characteristically decrease with fatigue, but are also affected by changes during dynamic contractions in 1) the relative positions of fibres and 2) the tissue filter effect. These effects make it sometimes impossible to track fatigue under dynamic conditions with power spectral parameters. In this investigation, tracking fatigue with CV was considered as an alternative to tracking fatigue with power spectral parameters.

The results of Experiment 1 indicated that CV estimation with a lone pair of single differential electrode channels was problematic at joint angles which coincided with maximal shortening of muscle fibres, regardless of force level. Results of the simulations indicated that the problems accounted for by end-effects could be reduced sufficiently by implementing a double differential electrode configuration and carefully selecting channel locations. The simulation also indicated however, that problems accounted for by electrodes traversing the IZ may not be so easily controlled.

The degree to which the traversing problem affects CV estimates is coupled to the amount of IZ migration that occurs as joint angle changes. Results from

Experiment 2 indicate that IZ migration occurs sufficiently to warrant concern. If the muscle of interest is pre-analyzed at extreme joint angles, an electrode location may be available that avoids the region which risks these electrode misplacement effects. However, such a location may not always be available and, in such cases, estimating CV with one pair of differential electrode channels is impractical.

Using an electrode array together with a gating algorithm may provide a solution to the problems associated with IZ migration. It is unlikely that an IZ would encompass the entire range of electrode channels in an array, so selective use of the channels could avoid using poor signals to estimate CV. Of course, this solution adds complexity to the measurement and estimation process, and in cases which demonstrate multiple IZs, may still lead to problematic CV estimation. While this technique is worth investigating, the added complexity renders it inappropriate for this work. Thus, results of this investigation indicate that until CV estimation techniques are sufficiently refined, CV is not a practical MES parameter for fatigue assessment.

## REFERENCES


1. S Johansson, LE Larsson, R Ortengren, “An automatic method for the frequency analysis of myoelectric signals evaluated by an investigation of the spectral changes following strong sustained contractions”, Medical and Biological Engineering, 8(3), pp. 257-264, 1970.

2. L Lindstrom, R Kadefors, I Petersén, “An electromyographic index for localized muscle fatigue”, Journal of Applied Physiology: Respiratory and Environmental Exercise Physiology, 43(4), pp. 750-754, 1977.

3. SJ Petrofsky, AR Lind, “Frequency analysis of the surface electromyogram during sustained isometric contractions”, European Journal of Applied Physiology, 43(2), pp. 173-182, 1980.

4. B Bigland-Ritchie, EF Donovan, CS Roussos, “Conduction velocity and emg power spectrum changes in fatigue of sustained maximal efforts”, Journal of Applied Physiology, 51(5), pp. 1300-1305, 1981.

5. KR Mills, “Power spectral analysis of electromyogram and compound muscle action potential during muscle fatigue and recovery”, Journal of Physiology, 326, pp. 401-409, 1982.

6. CJ De Luca, MA Sabbahi, FB Stulen, G Bilotto, “Some properties of the median frequency of the myoelectric signal during localized muscle fatigue”, Biochemistry of Exercise, HK Knuttgen, JA Vogel, J Poortmans, Eds. 13, pp. 175-183 1983.

7. R Merletti, LR Conte, C Orizio, “Indices of Muscle Fatigue,” Journal of Electromyography and Kinesiology, 1(1), pp. 20-30, 1991.

8. CJ De Luca, “Myoelectrical manifestations of localized muscular fatigue in humans”, CRC Critical Reviews in Biomedical Engineering, 11(4), pp. 251-279, 1984.

9. T Moritani, M Muro, A Nagata, “Intramuscular and surface Electromyogram changes during muscle fatigue”, Journal of Applied Physiology, 60(4), 1179-1185, 1986.

10. M Naeije, H Zorn, “Relation between EMG power spectrum shifts and muscle fibre action potential conduction velocity changes during local muscular fatigue in man”, European Journal of Applied Physiology, 50, pp. 23 - 33, 1982.

11. AC Guyton, ***Human Physiology and Mechanisms of Disease***, 5th Ed, WB Saunders Company, Philadelphia, 1992.

12. V Basmajian, CJ De Luca, 1985.***Muscles Alive: Their Functions Revealed by Electromyography***, 5th Ed., Williams & Wilkins, Baltimore, USA, 1985.

13. T Masuda, H Miyano, T Sadoyama, "The position of innervation zones in the bicpeps brachhii investigated by surface electromyography," IEEE Transactions on Biomedical Engineering, 32(1), pp. 36-42, 1985.

14. P Lago, NB Jones, "Effect of motor unit firing time statistics on EMG spectra", Medical and Biological Engineering and Computing, 15, p. 648-655, 1977.

15. CJ De Luca, "A model for a motor unit train recorded during constant force isometric contractions," Biological Cybernetics, 19, pp. 159-167, 1975.

16. F Buchthal, P Pinelli, P Rosenfalk, "Action potential parameters in normal human muscles and their physiological determinants", Acta. Physiologica Scandinavica, 32, pp. 219-229, 1954.

17. HP Clamman, "Statistical analysis of motor unit firing patterns in human skeletal muscle," Journal of Physiology, 9, pp. 1233-1251, 1969.

18. ZS Pan, Y Zhang, P Parker, "Motor unit power spectrum and firing rate" Medical and Biological engineering and Computing, 27(1), pp. 14-18, 1989.

19. Parker et al, IEEE Proceedings, 1975.

20. P Gatev, T Ivanova, GN Gantchev, "Changes in the firing pattern of high-threshold motor units due to fatigue", Electromyography and Clinical Neurophysiology, 26(2), p. 83-93, 1986.

21. CJ De Luca, M Knaflitz, ***Surface Electromyography: What's New?***, CLUT, Torino, Italy, 1992.

22. S Haykin, ***Communication Systems***, John Wiley & Sons, Inc., New York, 1994.

23. JS Bendat, AG Piersol, ***Measurement and Analysis of Random Data***, John Wiley & Sons Inc., New York, 1968.

24. P Bonato, G Gagliati, M Knaflitz, "Analysis of surface myoelectric signals recorded during dynamic contractions", IEEE Engineering in Medicine and Biology, 15, pp. 102-111, 1996.

25. MG Hagg, "Interpretation of EMG spectral alterations and alteration indexes at sustained contractions," Journal of Applied Physiology, 73(4), pp. 1211-1217, 1992.

26. HJ Hermens, TAM van Bruggen, CTM Baten, WLC Rutten, HBK Boom, “The median frequency of the surface EMG power spectrum in relation to motor unit firing and action potential properties,” Journal of Electromyography and Kinesiology, 2(1), pp. 15-25, 1992.

27. CJ De Luca, “The use of surface electromyography in biomechanics,” Journal of Applied Biomechanics, 73(4), pp. 1211-1217, 1992.

28. AD Cechetto, PA Parker, RN Scott, “The effects of four time-varying factors on the mean frequency of a myoelectric signal,” Journal of Electromyography and Kinesiology, 11(5), pp. 347-354, 2001.

29. D MacIsaac, PA Parker, RN Scott, “Non-stationary myoelectric signals and muscle fatigue,” Methods of Information in Medicine, 39, pp. 125-129, 2000.

30. B Hudgins, PA Parker, RN Scott, “A new strategy for multifunction myoelectric control,” IEEE Transactions on Biomedical Engineering, 40(1), pp. 82-94, 1993.

31. KB Englehart, “Signal representation for classification of the transient myoelectric signal,” PhD Dissertation, University of New Brunswick, Fredericton, Canada, 1998.

32. RE Chalis, RI Kitney, “Biomedical signal processing part 3: The power spectrum and coherence function,” Medical and Biological Engineering and Computing, 29, pp. 225-241, 1991.

33. AV Oppenheim, RW Schafer, ***Digital Signal Processing***, Prentice Hall, New Jersey, 1975.

34. L Cohen, ***Time-frequency Analysis***, Prentice Hall, New Jersey, 1995.

35. S Qian, D Chen, ***Joint Time-frequency Analysis: Methods and Applications***, Prentice-Hall, New Jersey, 1996.

36. P Bonato, SH Roy, M Knaflitz, CJ De Luca, “Time-frequency parameters of the surface myoelectric signal for assessing muscle fatigue during cyclic dynamic contractions, ” IEEE Transactions on Biomedical Engineering, 48(7), pp. 745-753, 2001.

37. S Karlsson, J Yu, M Akay, “Time-frequency analysis of myoelectric signals during dynamic contractions: A comparitive study,” IEEE Transactions on Biomedical Engineering, 47(2), pp. 228-238, 2000.

38. M Knaflitz, P Bonato, “Time-frequency methods applied to muscle fatigue assessment during dynamic contractions,” Journal of Electromyography and Kinesiology, 9, pp. 337-350, 1999.

39. SH Roy, P Bonato, M Knaflitz, “EMG assessment of back muscle function during cyclical lifting,” Journal of Electromyography and Kinesiology, 8, pp. 233-245, 1998.

40. G Balestra, S Frassinelli, M Knaflitz, F Molinari, “Time-frequency analysis of surface myoelectric signals during athletic movement,” IEEE Engineering in Medicine and Biology Magazine, 20(6), pp. 106-115, 2001.

41. HI Choi, WJ Williams, “Improved time-frequency representation of multicomponent signals using exponential kernels,” IEEE Transactions on Acoutsics, Speech, Signal Processing, 37, pp. 862-871, 1989.

42. B Boashash “Note on the use of the Wigner distribution for time-frequency signal analysis,” IEEE Transactions on Acoustics, Speech, Signal Processing, 36(9), pp. 1518-1521, 1988.

43. E Asmusson, “Muscle fatigue”, Medicine and Science in Sports, 11, pp. 313-321, 1979.

44. H Gibson, RHT Edwards, “Muscular exercise and fatigue”, Sports Medicine, 2, pp. 120-132, 1985.

45. E Hultman, H Sjoholm, “Biochemical causes of fatigue”, in ***Human Muscle Power***, NL Jones, NM Cortney, AJ McComas, (Eds.), Champaign, IL, Human Kinetics, pp. ??-??, 1986.

46. B Bigland-Ritchie, “Changes in muscle contractile properties and neural control during human muscular fatigue”, Muscle and Nerve, 7, pp. 691-699, 1984.

47. RM Enoka, “Neurobiology of Muscle Fatigue”, Journal of Applied Physiology, 72(5), pp. 1631-1648, 1992.

48. DT Kirkendall, “Mechanisms of peripheral fatigue”, Medicine and Science in Sport and Exercise, 22(4), pp. 444 - 449, 1990.

49. D Roberts, DJ Smith, “Biochemical aspects of peripheral muscle fatigue: a review”, Sports Medicine, 7, pp. 125-138, 1989.

50. K Sahlin, “Metabolic factors in fatigue”, Sports Medicine, 13(2), pp. 99-107, 1992.

51. DPM Maclaran, H Gibson, M Parry-Billings, RHT Edwards, “A review of metabolic and physiological factors in fatigue”, Exercise and Sport Sciences Reviews, 17, pp. 29-66, 1989.

52. LH Boobis, “Metabolic aspects of fatigue during sprinting”, in ***Exercise: Benefits, Limits and Adaptations***, D Macleod, R Maughan, M Nimmo, T Reilly, C Williams, (Eds.), E & FN Spon, London, 1987.

53. MJ Dawson, DG Gadian, DR Wilkie, “Muscular fatigue investigated by phosphorous nuclear magnetic resonance”, Nature, 274, pp. 861-866, 1978.

54. BD Ross, GK Radda, DG Gadian, G Rocker, M Esiri J Falconer-Smith, “Examination of a case of suspected Mcardles syndrome by nuclear resonance”, New England Journal of Medicine, 304, pp. 1338-1342, 1981.

55. RV Edgerton, B Saltin, B Esen, DR Simpson, “Glycogen depletion in specific types of human skeletal muscle fibres after various work routines”, International Symposium in Biochemistry of Exercise, pp. ??-??, Magglingen, 1973.

56. L Hermansen, O Vaague, “Lactate disappearance and glycogen synthesis in humans after maximal exercise”, American Journal of Physiology, 233, pp. 422-429, 1977.

57. HJ Green, “Neuromuscular aspects of fatigue”, Canadian Journal of Sports Science, 12(1), pp. 7s-19s, 1987.

58. SJ Petrosfsky, CA Phillips, “The physiology of static exercise”, Exercise and Sport Science Reviews, 14, pp. 1-44, 1986.

59. AE Spruce, NB Standen, PR Stanfield, “Voltage-dependant ATP sensitive potassium channels of skeletal muscle membrane”, Nature, 316, pp. 736-738, 1985.

60. D Chasiotis, K Sahlin, E Hultman, “Regulation of glycogenesis in human muscle at rest and during exercise”, Journal of Applied Physiology: Respiration and Environmental Exercise Physiology, 53, pp. 708-715, 1982.

61. K Sahlin, RC Harris, E Hultman, “Creatine kinase equillibrium and lactate content compared with muscle ph in tissue obtained after isometric exercise”, Biochemical Journal, 152, pp. 173-180, 1975.

62. P Tesch, B Sjodin, A Thorstenson, J Karlsson, “Muscle fatigue and its relation to lactate accumulation and LDH activity in man.”, Acta. Physiologica Scandinavica, 103, pp. 413-420, 1978.

63. G Miller, D Giannini, H Milner-Brown, R Layzer, A Koetsky, “Effects of fatiguing exercise on Hogh-energy phosphates, force and EMG: Evidence for three phases of recovery”, Muscle and Nerve, 10, pp. 810-821, 1987.

64. SH Roy, ER Boer, LD Gilmore, M Hrovat, “Concurrent measurement of muscle fatigue by EMG and 31P-NMR spectrascopy”, Electromyographical Kinesiology, pp. 279-181, 1991.

65. L Brody, M Pollock, S Roy, B Celli, CJ De Luca, “Effects of bath pH on EMG median frequency and conduction velocity in the hamster diaphragm”, Electromyographical Kinesiology, pp. 267-268, 1991.

66. P Orchardson, “The generation of nerve impulse in mammalian axons by changing the concentrations of the normal constituents of extracellular fluid”, Journal of Physiology, 275, pp. 177-189, 1987.

67. A Fabiato, F Fabiato, “Effects of pH on the myofilaments and the sarcoplasmic reticulum of skinned cells from cardiac and skeletal muscles”, Journal of Physiology, 276, pp. 233-255, 1978.

68. A Belchastro, I Mclean, J Gilchrist, “Biochemical basis of muscular fatigue associated with repetitious contractions of skeletal muscle”, International Journal of Biochemistry, 17, pp. 447-453, 1985.

69. C Bianchi, S Narayan, “Muscle fatigue and the role of transverse tubules”, Science, 215, pp. 295-296, 1982.

70. P Golnick, R Armstrong, W Sembrowich, R Shepard, B Saltin, “Glycogen depletion pattern in human skeletal muscle fibres after heavy exercise”, Journal of Applied Physiology, 34, pp. 615-618, 1973.

71. J Karlsson, “Lactate and phosphagen concentrations in working muscles of man”, Acta Physiologica Scandinavia, Suppl. 358, pp. 1-72, 1971.

72. JE Wilkerson, DL Batterton, SM Horvath, “Exercise induced changes in blood ammonia levels in humans”, European Journal of Applied Physiology, 37, 255-263, 1977.

73. BA Mutch, EW Banister, “Ammonia metabolism in exercise and fatigue: A review”, Medical Science and Sports Exercise, 15, pp. 41-50, 1983.

74. DE Heald, “Influence of ammonium ions on mechanical and electrophysiological responses of skeletal muscle”, American Journal of Physiology, 229, pp. 1174-1179, 1975.

75. G Sjogaaard, “Muscle energy metabolism and electrolyte shifts during low-level prolonged static contraction in man”, Acta Physiologica Scandinavica, 134, pp. 181-187, 1988.

76. J Scherrer, A Bourguignon, “Changes in the electromyogram produced by fatigue in man,” American Journal of Physical Medicine, 38, pp. 148-157, 1959.

77. OCJ Lippold, JWT Redfrearn J Vuco, “The electromyography of fatigue,” Ergonomics, 3 pp. 121-129, 1960.

78. HA Devries, “Efficiency of electrical activity as a physiological measure of the functional state of muscle tissue,” American Journal of Physical Medicine, ? pp. 47-52, 1968.

79. AJ Lloyd, “Surface electromyography during sustained isometric contractions,” Journal of Applied Physiology, 30, p. 713-722, 1971.

80. B Maton, “Human motor unit activity during the onset of muscle fatigue in submaximal isometric, isotonic contractions,” European Journal of Applied Physiology, 46(3), pp. 271-281, 1981.

81. B Bigland-Ritchie, JJ Woods, “Changes in muscle contractile properties and neural control during human muscular fatigue,” Muscle and Nerve, 7, pp. 691-699, 1984.

82. CJ De Luca, AM Roy, Z Erim, “Synchronization of motor-unit firings in several human muscles,” Journal of Neurophysiology, 70(5), pp. 2010-2022, 1993.

83. L Lindstrom, “On the frequency spectrum of EMG Signals,” PhD Dissertation, Chalmers University of Technology, Sweden, 1970.

84. R Merletti, M Knaflitz, CJ De Luca, “Electrically evoked myoelectric signals,” CRC Critical Reviews in Biomedical Engineering, 19, pp. 293-340, 1992.

85. W Linssen, D Stegman, E Joosten, M Vanthof R Binkhorst, S Noterman, “Variability and interrelationship of surface EMG parameters during local muscle fatigue,” Muscle and Nerve, 16, pp. 849-856, 1993.

86. H Broman, G Billoto, CJ De Luca, “A note on the non-invasive estimation of muscle fibre conduction velocity,” IEEE Transactions on Biomedical Engineering 32(5), pp. 341-344.

87. L Arendt-Nielsen, KR Mills, “The relationship between mean power frequency of the EMG spectrum and muscle fibre conduction velocity,” Electroencephalography and Neurophysiology, 60, pp. 130-134, 1985.

88. J Nyland, “Relation between local muscular fatigue and the EMG signal with emphasis on power spectral changes,” Isokinetic and Exercise Science, 3(4), pp. 171-180, 1993.

89. D MacIsaac, PA Parker, RN Scott, “The short-time Fourier transform and muscle fatigue assessment in dynamic contractions,” Journal of Electromyography and Kinesiology, 11, pp. 439-449, 2001.

90. JS Petrofsky, “Frequency and amplitude analysis of the EMG during exercise on the bicycle ergonometer,” European Journal of Physiology, 41, pp. 1-15, 1979.

91. FB Stulen, CJ De Luca, “Frequency parameters of the myoelectric signal as a measure of muscle conduction velocity,” IEEE Transactions on Biomedical Engineering, 28, pp. 515-523, 1981.

92. T D’Allesio, “Objective algorithm for maximum frequency estimation in Doppler spectral analyzers,” Medical and Biological Engineering and Computing, 23, pp. 63-68, 1985.

93. S Conforto, T D’Alessio, “Real time monitoring of muscular fatigue from dynamic surface myoelectric signals using a complex covariance approach,” Medical Engineering and Physics, 21, pp. 225-234, 1999.

94. DA Gabriel, JR Basford, KN An, “Assessing Fatigue with Electromyographic Spike Parameters,” IEEE Engineering in Medicine and Biology Magazine, 20(6), pp. 90-96, 2001.

95. DF Lovely, “Low noise electrode amplifier for use in evoked potential studies,” Canadian Medical and Biological Engineering Society Conference Proceedings, Ottawa, pp. 237-238, 1993.

96. SH Roy, CJ De Luca, J Schneider, "Effects of electrode location on myoelectric conduction velocity and median frequency estimates," Journal of Applied Physiology, 61 pp. 1510-1517, 1986.

97. R Merletti, SH Roy, E Jupa, R Silvestro, A Granata, “Modeling of surface myoelectric signals - Part II: model-based signal interpretation,” IEEE Transactions on Biomedical Engineering, 46(7), pp. 821-829, 1999.

98. A Rainoldi, M Naxxaro, R Merletti, D Farina, I Caruso, S Gaudenti, “Geometrical factors in surface EMG of the vastus medialis and lateralis muscles,” Journal of Electromyography and Kinesiology, 10, pp. 327-336, 2000.

99. D Farina, R Merletti, M Nazzaro, I Caruso, “Efffect of joint angle on EMG variables in leg and thigh muscles,” IEEE Transactions in Medicine and Biology, 20(6), 2001.

100. J Duchene, JY Hogrel, JF Marini, "Optimal protocol for muscle fiber conduction velocity estimation", Proceedings of the IEEE Engineering in Medicine and Biology Society/Canadian Engineering in Medicine and Biology Society Conference, pp. 1333-1334, 1995.

101. JA Gonzalez-Cueto, PA Parker, "Deconvolution estimation of motor unit conduction velocity distribution", IEEE Transactions on Biomedical Engineering …(get rest of reference)

102. R Plonsey, “The active fiber in a volume conductor,” IEEE Transactions on Biomedical Engineering, BME-12(?), pp. 371-381, 1974.

103. CJ De Luca, “Physiology and mathematics of myoelectric signals,” IEEE Transactions on Biomedical Engineering, IBME-26(6), pp. 313-325, 1979.

104. WS Masland, D Sheldon, CD Hershey, “The stochastic properties of individual motor unit interspike intervals,” American Journal of Physiology, 217, pp. 1384-1388, 1969.

105. RS Person, LP Kudina, “Discharge frequency and discharge pattern in human motor units during voluntary contractions of muscle,” Electroencephalography and Clinical Neurophysiology, ? pp. 471-483, 1972.

106. KC McGill, ZC Lateva, S Xiao, “A model of the muscle action potential for describing the leading edge, terminal wave, and slow afterwave,” IEEE Transactions on Biomedical engineering, 48(12), pp. 1356-1365, 2001.

107. GV Dimitrov, NA Dimitrova, “Fundamentals of power spectral of extracellular potentials produced by a skeletal muscle fibre of finite length. Part I: Effects of fibre anatomy,” Medical Engineering & Physics, 20(8), pp. 580-587, 1998.

108. EJ van Zulen, A van Velzen, JJ Denier van der Gon, “A biomechanical model for flexion torques of human arm muscles as a function of elbow angle,” Journal of Biomechanics, 21(3), pp. 193-190, 1988.